J. Phys. D: Appl. Phys. 24 (1991) 1025–1048. Printed in the UK

REVIEW ARTICLE

# Plasma sources based on the propagation of electromagnetic surface waves

**M Moisan and Z Zakrzewski†**

Département de Physique, Université de Montréal, Montréal, Québec H3C 3J7, Canada

Received 11 July 1990, in final form 28 January 1991

**Abstract.** Microwave and RF plasmas are finding increasing use in materials processing, plasma chemistry, chemical analysis, and other fields. This is stimulating the search for suitable plasma sources. In the 1970s, electromagnetic surface waves were put to use to sustain plasmas and an efficient microwave device, called a surfatron, was developed for this purpose. Recent work has shown that such discharges can also operate at radio frequencies. A large number of on surface-wave plasmas experimental data have been accumulated—their modelling is well advanced and they have found applications in various fields of research and technology.

This paper reviews the physical principles of operation and the design of surface-wave plasma sources. Since the wave launcher is the central component of the source, this review presents a unified description of several compact, efficient, and easy to operate launchers specifically intended for plasma generation that have been developed over the past fifteen years. It is now possible to sustain such plasmas at frequencies ranging from 1 MHz to 10 GHz, in a pressure domain extending from $10^{-5}$ Torr up to few times atmospheric pressure, and in a rich variety of plasma vessels and reaction chambers.

## 1. Introduction

During the last few decades, the use of microwave and RF discharges, henceforth jointly referred to as high-frequency (HF) discharges, has greatly expanded. One reason is the continuous progress in the availability of RF and microwave power hardware, and the lowering of its cost. Also, researchers and engineers now realise that relative to the various DC discharges, HF discharges, in particular the microwave ones, are generally less expensive, easier to handle, more efficient, and more reliable sources of particles and radiation for physical studies and technical applications (see e.g. Hollahan and Bell 1974, MacDonald and Tetenbaum 1978).

For decades HF discharges were, and still are, mostly maintained either between metal electrodes (located inside or outside the discharge vessel) or within coils and resonant cavities. Only recently has a qualitatively new way of producing HF plasmas been proposed that removes some of the shortcomings of the already existing RF and microwave plasmas. This consists in using electromagnetic surface waves to sustain the discharge. The fact that a (non-ionizing) surface wave can propagate along the interface between a plasma column and its surrounding dielectric tube has been known since the 1960s (Trivelpiece and Gould 1959, Trivelpiece 1967). (For reviews of this subject see Shivarova and Zhelyazkov (1978) and Moisan *et al* (1982a) on theory and experiment respectively.) In the 1970s, the interest in such waves shifted to their use as a means of sustaining a plasma column. Tuma (1970) was probably the first to identify a surface-wave-produced discharge clearly. Moisan *et al* (1974, 1975, 1979a) developed the surfatron, which was the first simple, compact, and efficient surface-wave launcher for the generation of long plasma columns at microwave frequencies. The properties of the wave sustaining such plasma columns were then investigated by Zakrzewski *et al* (1977) who measured its dispersion and attenuation characteristics.

Recent progress with surface-wave launchers extends the use of surface-wave discharges (SWDs) from

† Permanent address: Polish Academy of Sciences, IMP-PAN, 80-952 Gdansk, Poland.

0022-3727/91/071025 + 24 $03.50 

the microwave to the RF range (Moisan and Zakrzewski 1987), the operating frequency band now running from less than one MHz up to 10 GHz. The fact that the same field configuration can be used to produce plasmas in this broad frequency range is a unique feature of surface-wave plasmas that has proved useful in the investigation of the frequency optimization of HF plasma processes (Moisan *et al* 1991). It must also be pointed out that there exist large numbers of experimental data on these plasmas, and their modelling is well advanced. This provides a rather unified and complete picture of their properties. Moreover, such an insight has led to a better understanding of the physical processes of electrodeless HF discharges in general and to a corresponding simplified general model (Moisan and Zakrzewski 1986).

Many reviews of the properties and applications of surface-wave produced plasmas can be found (Marec *et al* 1982, Moisan *et al* 1982b, Moisan and Zakrzewski 1986, Chaker *et al* 1986). These plasmas are characterized by an unusual flexibility in operating conditions. For example, depending on the tube radius, they have been produced at gas pressures as low as some $10^{-5}$ Torr up to a few times atmospheric pressure. It is noteworthy that discharge tubes with diameters ranging from 0.5 mm to 150 mm have been used (larger diameter vessels are less common, and thus more costly). The surface wave can be excited by a very compact wave launcher which needs to surround only a small portion of the discharge vessel, the HF power being carried to the rest of the column by the propagating wave. The plasmas obtained are stable, they are reproducible because monomode wave propagation can be achieved, and they are quiescent, the level of the electron density fluctuations being low. The properties of the SWD depend only on the amount of power absorbed per unit length of the plasma and on the *discharge conditions*†, namely the composition and the pressure of the gas, the dimensions of the discharge tube and the wall material, the wave mode and the frequency. Note that these properties are independent of the type of wave launcher used.

The SWD has found many applications, some of which are well documented: materials processing (Loncar *et al* 1980, Paquin *et al* 1985, Paraszczak *et al* 1985, Claude *et al* 1987, Sauvé *et al* 1988), ion sources (Henry *et al* 1983, Pomathiod *et al* 1988), lasers (Bertrand *et al* 1978, 1979, Waynant *et al* 1985, Bollen *et al* 1985, Moutoulas *et al* 1985), elemental analysis (Hubert *et al* 1979, Moisan *et al* 1979b, Hanai *et al* 1981, Abdallah *et al* 1982, Chevrier *et al* 1982, Hubert *et al* 1986, Deruaz and Mermet 1986, Selby and Hieftje 1987, Selby *et al* 1987, Rivière *et al* 1987, Galante *et al* 1988, Besner *et al* 1988) and lighting (Beauchemin *et al* 1986, Beneking and Anderer 1987, Levy 1990, Margot *et al* 1991).

Although the specific design of the wave launcher does not affect the plasma parameters, the launcher plays an essential part in the plasma source set-up: it determines the efficiency of the power transfer from the power generator to the plasma and, to some extent, it imposes the wave propagation mode. For simplicity, we refer only to low-pressure surface-wave plasmas. However, all the wave launchers described here can efficiently produce discharges up to pressures exceeding one atmosphere. This is the case, for example, in most of the elemental analysis applications quoted above. The differences are in the plasma properties and in the methods of plasma modelling, and not in the launcher design or in the operational procedures (Moisan *et al* 1990, Nowakowska *et al* 1990).

This review is organised as follows. Section 2 contains a short review of the principal physical processes in a low gas pressure SWD, with the corresponding modelling. In section 3, we concentrate on specific aspects of the launching and propagation of a surface wave that sustains a discharge. Section 4 is devoted to the description of a family of launchers whose individual frequency domain can be summed up to generate a plasma efficiently over the full range of frequencies mentioned. Section 5 examines the various components that, together with the wave launcher, form a SWD plasma source.

## 2. The physics and modelling of low-pressure surface-wave sustained plasmas

### 2.1. Power balance in a steady-state travelling-wave discharge

Discharges sustained by surface waves belong to the general category of travelling wave discharges (TWDS) (see e.g. Moisan and Zakrzewski 1986). Because of their specific mechanism of energy transfer from the electromagnetic field to the plasma, these discharges exhibit features that set them apart from conventional discharges sustained within HF circuits. Therefore, before addressing the question of surface-wave launchers, we start with a short summary of the basic aspects of TWDS.

Consider a HF discharge sustained in a cylindrical, dielectric vessel by the field of an electromagnetic wave propagating along it. The length of the *active zone* of the discharge, i.e. the region where the HF power transfers to the plasma, is large compared with its diameter. The wave is launched at axial position $z = 0$ (figure 1) and propagates in the $z$ direction. The power flux of the wave decreases with increasing $z$ as power is gradually expended in sustaining the discharge. The column ends at $z = l$, where the wave power drops below the level necessary to sustain the plasma. Because the power dissipated per unit length of the plasma column varies along the axis of the vessel, so do some of the parameters of the plasma. As an example, we have sketched in figure 1 the axial distribution of the cross section average electron density.

† We draw the reader's attention to this definition of discharge conditions that shall be used throughout the review.

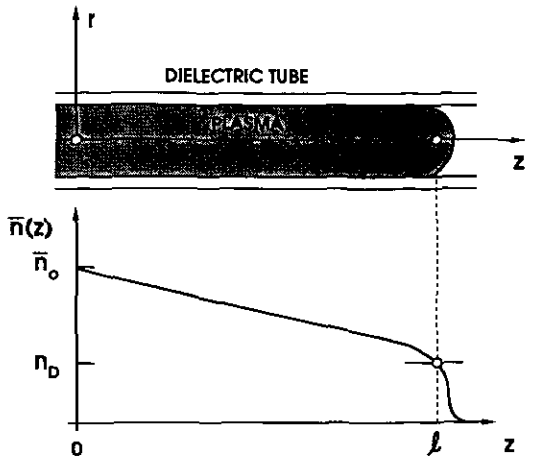


**Figure 1.** The plasma column, the cylindrical coordinates adopted, and the axial distribution of the cross section average electron density. The axial position $z = l$ where the electron density suddenly collapses is called the end of the plasma column; the corresponding electron density is $n_D$.

To establish the conditions of existence of a steady-state TWD, we now turn to the analysis of its power balance. For simplicity, assume as a first approximation, that the influence of any axial gradient, as far as the discharge processes and the wave propagation are concerned, is negligible. This means that there is no net exchange of power between consecutive elementary sections along the plasma column, and the power balance may thus be considered separately for each section. Furthermore, the analysis of a given TWD segment $z$, $z + \Delta z$ is the same as that for a uniform discharge, this assumption being usually referred to as the local uniformity approximation.

The amount of power entering the plasma, and thus diverted from the main power flux $P(z)$ of the wave travelling along the discharge over the distance $z$, $z + dz$, can be expressed by defining the wave attenuation coefficient

$$\alpha(z) \equiv -\frac{1}{2}\frac{1}{P(z)}\frac{dP(z)}{dz}. \tag{1}$$

The power per unit length of the discharge channelled out of the main power flux $P(z)$ over the distance $z$, $z + dz$ is then

$$A(z) \equiv -\frac{dP(z)}{dz} = 2\alpha(z)P(z). \tag{2}$$

With TWDs, we assume that the power extracted from the wave between the planes $z$ and $z + \Delta z$ is transferred to the plasma within the corresponding elementary segment $z$, $z + \Delta z$ of the plasma column, as illustrated in figure 2. The power loss in the plasma can be expressed as Joule heating and we have†, under steady-state conditions

$$2\alpha(n)P(z)\Delta z = 2\pi\int_0^a \sigma(n)E^2(r)r\,dr\,\Delta z. \tag{3}$$

where $n$ is the electron density, $a$ is the inner radius of the tube, $\sigma(n)$ denotes the corresponding plasma electric conductivity, and $E(r)$ is the average total electric field strength of the wave, expressed as a function of the radial position $r$. Under given discharge conditions and to a first approximation (section 2.2.2), the attenuation coefficient depends only on the cross sectional average electron density $\bar{n}$. This density varies with $z$. We shall refer to $\alpha(\bar{n})$ as the attenuation characteristic of the wave.

When the field frequency exceeds a few MHz, practically all the power absorbed by the plasma is intercepted by the electrons. The power per unit length lost by the electrons through collisions of all kinds, and gained by heavy particles, is

$$L(\bar{n})\Delta z \equiv \pi a^2 \bar{n}\theta\Delta z \tag{4}$$

where $\theta$ is the power lost per electron. Ultimately, this power reaches the environment through optical radiation, particle–wall interactions, etc. When the electron energy distribution function (EEDF) is independent of the electron density‡ and provided that there is no step-wise excitation or ionization, $\theta$ is also density independent. As a consequence, $\theta$ (and thus $\bar{E}(z)$) is constant along the plasma column, except at the very end (Ferreira 1983, 1986, Moisan and Zakrzewski 1986, Ferreira and Moisan 1988).

Under steady-state conditions, the power balance relation in a TWD leads to $A(\bar{n}) = L(\bar{n})$, i.e.

$$2\alpha(\bar{n})P(z) = \pi a^2 \bar{n}\theta. \tag{5}$$

This condition must be fulfilled locally at any axial position along the discharge. Note that, in a steady-state discharge, $\theta$ is the power required to maintain an ion-electron pair in the plasma.

We now calculate the axial distribution of the electron density and of the wave power, assuming that $\alpha(\bar{n})$ is known. Taking the logarithmic derivative of both sides of equation (5) and recalling that $\theta$ is a constant with respect to $n$ and $z$, it follows that (Glaude *et al* 1980)

$$\frac{1}{\bar{n}(z)}\frac{d\bar{n}(z)}{dz} = -2\alpha(\bar{n})\left(1 - \frac{\bar{n}(z)}{\alpha(\bar{n})}\frac{d\alpha(\bar{n})}{d\bar{n}}\right)^{-1}. \tag{6}$$

This equation gives the axial distribution $\bar{n}(z)$ of the average electron density over a cross section. The

† Equation (3) assumes that the electric field strength $E$ does not vary with the azimuthal angle $\varphi$ (only true with the $m = 0$ mode wave, see section 2.2.1) and that $\sigma$ is a scalar (no externally applied magnetic field).

‡ This implies a diffusion-controlled discharge and rules out volume recombination of the charged particles as the main loss mechanism, as considered, for example, by Zhelyazkov *et al* (1986). It also assumes electron–neutron or electron–electron collisions to be dominating, excluding the transition between these two collisional regimes.

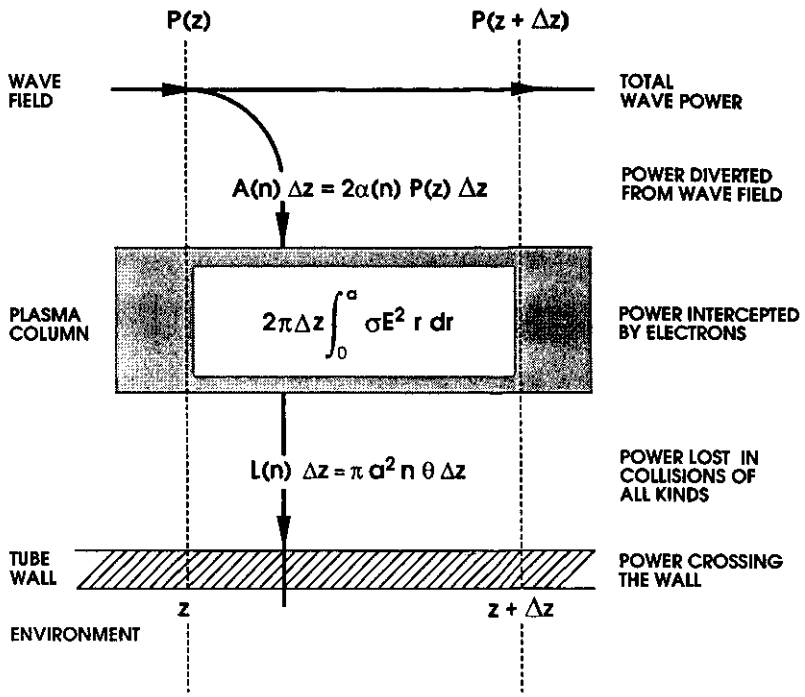


**Figure 2.** The power flow within an elementary axial segment of a plasma column sustained by a travelling wave.

boundary condition $\bar{n}(0) \equiv \bar{n}_0$ for this differential equation is set by the power $P(0) \equiv P_0$ at the launcher exit that is delivered to the whole plasma column, the value of $\bar{n}_0$ following from equation (5), as

$$2\alpha(\bar{n}_0)P_0 = \pi a^2 \bar{n}_0 \theta. \tag{7}$$

As for the axial distribution of the wave power, it is obtained from equations (5) and (7) as

$$\frac{P(z)}{P_0} = \frac{\alpha_0}{\alpha(\bar{n})}\frac{\bar{n}(z)}{\bar{n}_0} \tag{8}$$

where $\alpha_0 \equiv \alpha(\bar{n}_0)$.

The power balance condition (5) is necessary, but not sufficient, for a steady-state discharge to exist. Indeed, not only does the power lost by the electrons have to be compensated by the power transferred to the plasma by the electromagnetic field, but this power equilibrium has to be stable. This problem is usually connected with the fact that, for given values of $P(z)$ and $\theta$, equation (5) may have more than one solution for $\bar{n}$. Some of these solutions, and sometimes all of them, may be unstable at a given axial position $z$.

To illustrate this stability problem we shall consider a specific† function $\alpha(\bar{n})$, though the reasoning is general. Figure 3 shows a sketch of both power densities

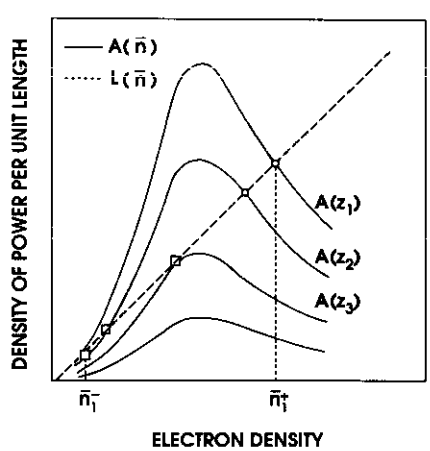


**Figure 3.** Stable (○) and unstable (□) local balance of power (equation (5)) in a low-collision steady-state travelling-wave discharge. $A(z_k)$ denotes the power per unit length of the discharge that can be channelled out of the main power flux $P(z)$ at the position $z_k$ depending on the value of $\bar{n}$ at that position. The function $L(\bar{n})$ represents the power lost by the electrons through collisions of all kinds. No discharge exists beyond $z_3$, where $z_3 > z_2 > z_1$, because the power flux $P(z)$ has dropped to too low a value.

$A$ and $L$ against $\bar{n}$. Under given discharge conditions the power-loss curve is a straight line. The various absorbed power curves $A(\bar{n}) = 2\alpha(\bar{n})P(z)$ shown in the figure differ only by the multiplying factor $P(z)$, the power flow at a distance $z$ from the launcher. We now consider what happens at $z = z_1$, where the power flow is $P(z_1)$. The possible electron density values there are given by the intersection of curves $A(z_1)$ and $L(\bar{n})$.

† The behaviour of the attenuation coefficient $\alpha(\bar{n})$ considered here corresponds to that of the forward wave domain of propagation in a low-collision cold plasma (Shivarova and Zhelyazkov 1978). The backward wave often gives rise to an $\alpha(\bar{n})$ curve going through a minimum rather than a maximum as a function of $\bar{n}$. Except possibly for a very limited electron density range, the backward wave generally leads to an unstable TWD. In section 2.2, we discuss only forward wave propagation and only the part that provides a stable SWD.

Two values of density are obtained in the present example but only those marked by open circles are stable, as we shall now see.

The discharge is stable if any random fluctuation of the electron density triggers a sequence of events that leads to the restoration of the original density. Consider for example a discharge in which a random decrease $\Delta n$ of the electron density occurs. This causes the values of $A$ and $L$ to change, and therefore destroys the existing balance of power. This balance is restored only provided the decrease in the initial electron density from $n_1$ to $n_1 - \Delta n$ corresponds to an absorbed power $A(n_1 - \Delta n, z_1)$ that exceeds the electron collisions power loss $L(n_1 - \Delta n)$, thus enhancing the creation of electrons. The opposite behaviour is required when the initial change is an increase of density. Therefore, in a stable steady-state discharge,

$$\frac{\mathrm{d}A(\bar{n})}{\mathrm{d}\bar{n}} < \frac{\mathrm{d}L(\bar{n})}{\mathrm{d}\bar{n}}. \tag{9}$$

This requirement is met at the crossing points marked by circles in figure 3. On the other hand, one may check that a random decrease in density initiated at a point (marked by a square) leads to the extinction of the discharge, while a random increase from that same point results in a steady growth of the electron density until it reaches one of the values marked by a circle, corresponding to a stable balance of power. Figure 3 shows that if $P(z)$ decreases, the value of the 'stable' density $\bar{n}$ decreases. Also, if $P(z)$ drops below a certain minimum value, there is no solution at all. A condition similar to equation (9) was formulated earlier by Taillet (1969) and Leprince *et al* (1971) for resonantly sustained plasmas.

Substituting equations (4) and (5) into the above inequality, one obtains the condition for a stable power balance in a TWD explicitly in terms of $\alpha(\bar{n})$, namely

$$\frac{\mathrm{d}\alpha(\bar{n})}{\alpha(\bar{n})} < \frac{\mathrm{d}\bar{n}}{\bar{n}}. \tag{10}$$

This criterion was first formulated by Zakrzewski (1983). It determines, through the allowed dependence $\alpha(\bar{n})$, the type of travelling wave that can be used to sustain a TWD as well as the range of electron density, and thus that of the wave power, over which a steady-state discharge can occur. Applying the stability criterion (10) to equation (6) yields the further condition $\mathrm{d}n/\mathrm{d}z < 0$, where $z$ is measured from the launcher exit.

It thus follows that the wave attenuation characteristic $\alpha(\bar{n})$ not only defines the axial distribution of the plasma parameters in the TWD, but also determines whether or not a steady-state discharge can exist.

## 2.2. Azimuthally symmetric surface waves along a uniform plasma column: theoretical summary of their properties

**2.2.1. Surface-wave modes.** A bounded plasma may support electromagnetic surface waves. These waves are guided along the boundary surface, where their energy flux is concentrated. As a rule, the plasma is contained within a cylindrical dielectric tube, which is sometimes placed coaxially within a metal enclosure. However, the metal-free configuration is the one most often used.

The modes of propagation of surface waves along a cylindrical medium are characterized by the factor $\exp(\mathrm{j}m\varphi)$ affecting the field intensity components, where $m$ is an integer, $\mathrm{j} = \sqrt{-1}$, and $\varphi$ is the azimuthal angle. The lowest order mode $m = 0$, for which the field is independent of $\varphi$, is the most commonly used; we therefore limit ourselves to that mode.

The results presented here also apply to an axially non-uniform plasma column, provided that the axial variation of the electron density is slow enough for the wave to see a locally uniform medium, which requires

$$\frac{1}{\bar{n}(z)}\left|\frac{\mathrm{d}\bar{n}(z)}{\mathrm{d}z}\right| \ll \beta \tag{11}$$

where $\beta$ is the phase coefficient, or axial wavenumber, of the surface wave.

**2.2.2. Phase and attenuation characteristics of the $m = 0$ surface wave.** It follows from the conclusion of section 2.1 that the main aspect of wave propagation to sustain a TWD is the attenuation characteristic $\alpha(\bar{n})$ of the wave. This function is easily obtained experimentally (Zakrzewski *et al* 1977, Glaude *et al* 1980, Moisan *et al* 1982b). It can also be calculated and different methods can be used (Glaude *et al* 1980, Zhelyazkov *et al* 1986, Granier *et al* 1987, Zhelyazkov and Benova 1989).

Our calculations of $\alpha(\bar{n})$ and $\beta(\bar{n})$ are valid whatever the value of the ratio of collision frequency to wave frequency, the dispersion relation being solved using complex algebra (Glaude *et al* 1980). Aside from the local axial uniformity approximation, it is also assumed that the radial distribution of electron density only reflects on $\beta$ and $\alpha$ through the value of the cross sectional average density $\bar{n}$. Theory shows that this latter assumption is fully justified, provided that $\beta a < 1$ (Trivelpiece 1967, Ferreira 1986). This has been verified experimentally (e.g. Moisan *et al* 1982b).

Defining the complex axial wavenumber $h = \beta + \mathrm{j}\alpha$, the axial component of the electric field strength for the $m = 0$ surface-wave mode in a cylindrical configuration, in the $k$th medium of relative permittivity $\varepsilon_k$, is

$$E_{zk} = A_k J_0[(\beta_0^2\varepsilon_k - h^2)^{1/2}r] + B_k H_0^{(1)}[(\beta_0^2\varepsilon_k - h^2)^{1/2}r] \tag{12}$$

where $J_0$ and $H_0^{(1)}$ are the zeroth-order Bessel and Hankel functions of the first kind respectively, $A_k$ and $B_k$ are constants to be determined from field continuity conditions at the boundary, and $\beta_0 = 2\pi/\lambda_0$, where $\lambda_0$ is the wavelength in free space. Note that the field components are complex functions of complex arguments. The sign of the square roots is chosen to make

the imaginary part of the argument positive. This restriction is necessary to obtain a zero field value from $H_0^{(1)}$ when $r$ tends to infinity. Additional conditions on the constants $A_k$ and $B_k$ are imposed by the fact that the electric field intensity must remain finite at $r = 0$ and must go to zero for $r$ tending to infinity, as already mentioned; in the case of a plasma tube surrounded by air, this corresponds to $B_k = 0$ in the plasma and $A_k = 0$ outside it, respectively. The remaining field components $E_{rk}$ and $H_{\varphi k}$ are directly related to $E_{zk}$ by the usual electromagnetic field relations. There are no other field components since the $m = 0$ surface wave is a TM wave.

The continuity requirement for the field components $E_{zk}$ and $H_{\varphi k}$ at the various interfaces provides a set of linear equations that has a non-trivial solution only if their characteristic determinant $D$ is zero. The condition $D(\omega/\omega_{pe}, \nu_{eff}, a; \alpha + j\beta) = 0$ for fixed $\omega$ (wave angular frequency), $\nu_{eff}$ (effective electron–neutral collision frequency for momentum transfer (Heald and Wharton 1965)) and $a$ (plasma radius), and for $\omega_{pe}$ varying†, yields $\beta + j\alpha$. That is, it yields two relations: firstly $\omega/\omega_{pe}$ against $\beta$, called the *phase characteristic* (we use this term in the case of fixed $\omega$, in contrast to the usual dispersion characteristic for which $\omega$ varies and $\omega_{pe}$ is fixed), and secondly $\omega/\omega_{pe}$ against $\alpha$, the *attenuation characteristic*. Henceforth, we shall refer to the functional dependences $\beta(\bar{n})$ and $\alpha(\bar{n})$ as the phase characteristic and attenuation characteristic of the wave respectively. These results are valid whatever the value of the plasma parameters and, in particular, whatever the value of $\alpha$ compared with $\beta$.

Figure 4 shows an example of the calculated phase characteristic for the azimuthally symmetric surface wave. At low gas pressures, i.e. under conditions such that $\nu_{eff}^2 \ll \omega^2$, the shape of the phase characteristic is practically independent of the value of $\nu_{eff}$ (Trivelpiece 1959). Figure 5 shows the attenuation characteristic of the wave under the same conditions as in figure 4. Still at low gas pressures, a satisfactory analytical approximation for $\alpha(\bar{n})$ is (Zakrzewski and Moisan 1986)

$$\alpha(\bar{n}) = \frac{B(\omega, a)\nu_{eff}}{\bar{n} - n_D} \qquad (13)$$

where $n_D$ is the electron density‡ corresponding to the surface-wave resonance ($\beta \to \infty$); $B(\omega, a)$ has to be determined by fitting equation (13) to the attenuation characteristic computed for a given $\omega$ and $a$. The effective electron collision frequency $\nu_{eff}$ depends on the nature of the gas and, to some extent, is proportional to its pressure. Note that equation (13) implies that $\bar{n} > n_D$ (and so $n_D$) defines the end of the plasma column. The above analytical expression displays in an explicit way the influence of the discharge conditions and plasma parameters on the attenuation coefficient. In particular, it shows that $\alpha(\bar{n})$ increases with decreasing electron density.

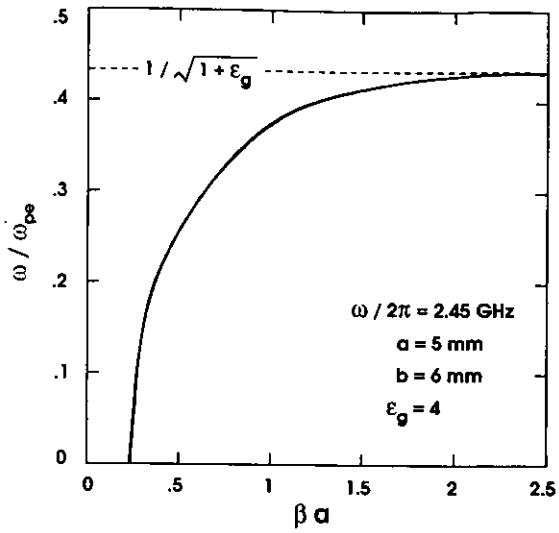


**Figure 4.** Calculated phase characteristic for the $m = 0$ mode surface wave (forward wave domain, $\nu_{eff} \ll \omega$). $\beta$ is the surface-wave wavenumber along $z$, $a$ is the plasma radius, $b$ is the discharge tube outer radius, $\omega$ and $\omega_{pe}$ are the wave and electron plasma angular frequency respectively, and $\varepsilon_g$ is the tube relative permittivity.

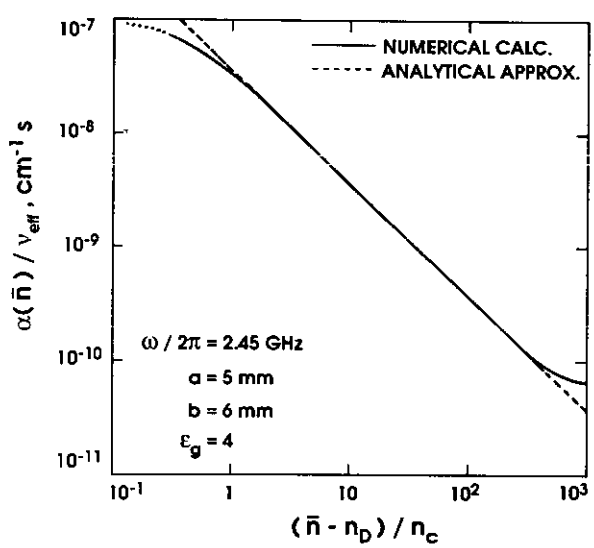


**Figure 5.** Calculated attenuation characteristic for the $m = 0$ mode surface wave (forward wave domain, $\nu_{eff} \ll \omega$) and its analytical approximation by equation (13) with $B(\omega, a) = 3.7 \times 10^{-8}$ cm$^{-4}$ s. The wave attenuation coefficient $\alpha(\bar{n})$ is a function of the cross sectional average electron density, $\nu_{eff}$ is the effective electron–neutral collision frequency for momentum transfer, $n_c$ is the critical electron density ($\omega = \omega_{pe}$), and $n_D$ is the density at the end of the column. Conditions for the wave propagation are the same as in figure 4.

† The electron plasma (angular) frequency $\omega_{pe} = (ne^2/\varepsilon_0 m_e)^{1/2}$ depends only on the value of the electron density $n$ ($e$ and $m_e$ are the electron charge and mass respectively; $\varepsilon_0$ denotes the permittivity of free space). A complementary relation, namely $\omega = \omega_{pe}$, defines the so-called critical electron density $n_c$ as given by $\omega = (n_c e^2/\varepsilon_0 m_e)^{1/2}$. Note that $\omega^2/\omega_{pe}^2 = n/n_c$.

‡ In the cold plasma approximation and for $\nu_{eff} \ll \omega$, $n_D = (1 + \varepsilon_g)n_c$, where $\varepsilon_g$ is the relative permittivity of the tube wall and $n_c$ is the critical density (see preceding footnote). For values of the electron density that are too close to $n_D$, approximation (13) is no longer valid. It can however be shown that in fact $\alpha(\bar{n})$ reaches its maximum value at approximately that density.

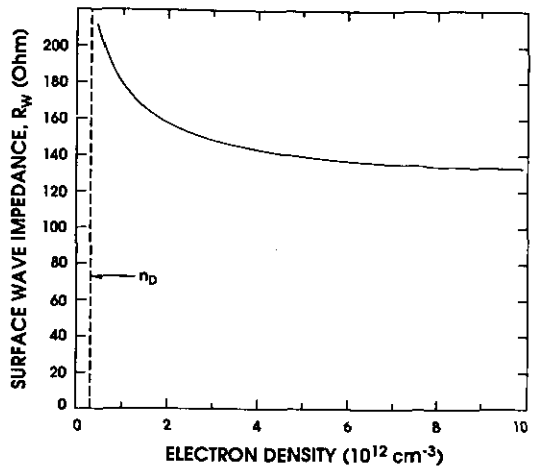


**Figure 6.** Calculated characteristic impedance $R_w$ of the plasma column as a function of electron density, as seen by the $m = 0$ mode surface wave at 2450 MHz in a fused silica ($\varepsilon_g = 3.78$) discharge tube of 10 mm ID and 12 mm OD.

**2.2.3. Characteristic impedance of the plasma column for the $m = 0$ surface wave.** Another parameter of interest for surface-wave propagation is the characteristic impedance $R_w$ presented by the plasma column to the wave. As we shall show in section 3, this impedance is instrumental in the description of the energy transfer process from the wave launcher to the excited wave. The characteristic impedance $R_w$ can be defined as

$$R_w = U^2/2P \tag{14}$$

with

$$U = \int_0^\infty E_r(r)\,\mathrm{d}r \tag{15}$$

where $E_r(r)$ is the radial component of the wave's electric field strength and $P$ is the total (i.e. including all media) power flux of the wave at $z$. In the case of a weakly attenuated wave the characteristic impedance can be taken to be real. Recall that the characteristic impedance for any wave other than transverse electric and magnetic (TEM) waves cannot be uniquely defined. We have chosen the definition (14) and (15) because it yields a value of $R_w$ that can be used in our equivalent circuit representation of the wave launchers, to account for the power carried away by the wave. Figure 6 shows a typical example of the dependence of $R_w$ on $\bar{n}$. Note that, for electron density values exceeding a few times the resonance density $n_D$, the plasma impedance seen by the wave is nearly independent of $\bar{n}$. This stability of the impedance under possibly varying discharge conditions may be important for certain applications, such as analytical chemistry, as it means that the impedance matching of the plasma source with the HF generator then remains unaffected.

### 2.3. Charged particle balance and the power loss per electron in a low-pressure steady-state discharge

**2.3.1. Charged particle balance.** This section concerns discharges sustained in a pressure range including, on the high-pressure side, the ambipolar diffusion regime and, on the low-pressure side, the free-fall regime. It summarizes the theoretical work on the charged particle balance and the power loss per electron $\theta$ in HF discharges (for an extensive review see Ferreira and Moisan 1988).

Let us start with the charged particle balance. Self and Ewald (1966) proposed a two-moment theory that covers both the ambipolar diffusion regime and the free-fall regime, as well as the transition between these two regimes. Later, Ingold (1978) showed that a good approximation to the exact theory of Self and Ewald could be obtained by solving a diffusion-type continuity equation. For cylindrical geometry, the radial profile of the electron density, as calculated with Ingold's approximation, is given by

$$n(r) = n_A J_0(r/\Lambda_e) \tag{16}$$

where $n_A$ is the density at the tube axis, and $\Lambda_e$ is an effective diffusion length defined by

$$\Lambda_e^{-2} = (1 + 2\langle\nu_i\rangle/\nu_{in})\langle\nu_i\rangle/D_a. \tag{17}$$

In the above, $\nu_i$ is the collision frequency for ionization by electron impact, $\nu_{in}$ is the average collision frequency of ions with neutrals, and $D_a$ is the ambipolar diffusion coefficient. The brackets $\langle\ \rangle$ denote averaging over the electron energy distribution function.

The Ingold formulation also yields the indicial relation

$$\frac{J_0(a/\Lambda_e)}{(a/\Lambda_e)} = \left(\frac{\langle\nu_i\rangle}{\nu_{in} + 2\langle\nu_i\rangle}\right)^{1/2} \tag{18}$$

which, together with equation (16), gives the radial distribution of the electron density. Combined with equation (17) it leads to the average value of the electron energy. With the latter value at hand one can address the question of the power loss per electron.

**2.3.2. The power loss per electron.** The energy lost by an average electron in collisions of all kinds is given approximately by

$$\theta \simeq (2m_e/M)\langle\nu_e\varepsilon\rangle + \sum_j \langle\nu_j\rangle eV_j + \langle\nu_i\rangle eV_i \tag{19}$$

where $M$ is the atomic or molecular mass, $\nu_e$ is the microscopic electron–neutral collision frequency for momentum transfer, $\nu_j$ is the collision frequency for the excitation of atoms or molecules to energy level $j$ by electron impact (Ferreira and Loureiro 1984), and $\varepsilon = m_e w^2/2$ is the electron kinetic energy. The quantities $eV_i$ and $eV_j$ are the threshold energy values for ionization and excitation by electron impact respectively. Recall that we assume operating conditions such that $\theta$ is density independent (see footnote after equation (5)).

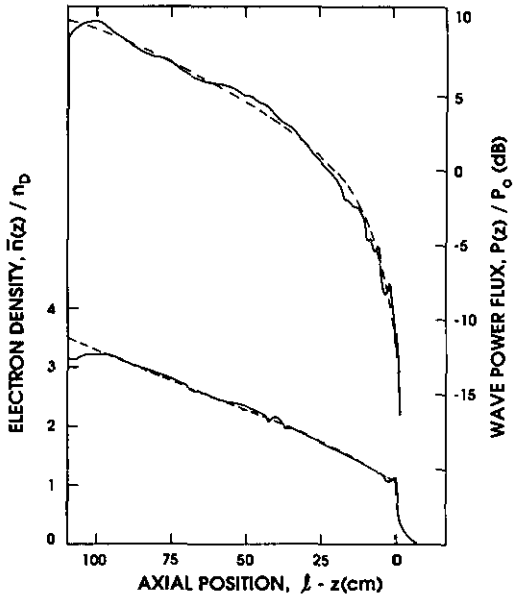


**Figure 7.** Experimental (full curve) and theoretical (broken curve) axial dependence of the wave power flux and electron density in a surface-wave discharge of length $l$ at 700 MHz and 20 mTorr of argon, in a Pyrex ($\varepsilon_g = 4.5$) discharge tube with 22.2 mm ID and 27.4 mm OD. The electron density is normalized to the surface-wave resonance density $n_D = 3.4 \times 10^{10}\,\mathrm{cm}^{-3}$, whereas the wave power flux $P(z)$ is normalized to its value $P_0$ at the launcher gap.

## 3. General conditions for the launching and the propagation of a surface wave sustaining a discharge

### 3.1. Some characteristics of SWDs

**3.1.1. Spatial distribution of the electron density.** There is an essential difference between the situation in which the surface wave propagates along a plasma column created by some other means (for example, the positive column of a DC discharge) and the situation in which the wave itself sustains the plasma. This difference follows from the fact that, in the latter case, the discharge depends on the wave and conversely. Under steady-state conditions, the plasma parameters at any position along the TWD are set self-consistently as a result of locally balancing the power lost by the electrons against the power acquired from the wave field. The outcome is the axial distribution of the electron density given by equation (6). Recall that on applying the stability criterion (10) to equation (6), one obtains that $dn(z)/dz < 0$. Therefore, axial non-uniformity of the plasma is an intrinsic feature of discharges sustained with surface waves in a travelling mode. This is illustrated in figure 7, which shows a typical example of the axial distribution of wave power and electron density in a SWD. The full curves show the experimental results (for details on the experimental set-up and procedure see Zakrzewski *et al* (1977)). The broken curves are best fits computed from equations (6) and (8), together with the analytical approximation (13) for the wave attenuation characteristic. There is only one fitting parameter for both curves, namely the effective collision frequency $\nu_{\mathrm{eff}}$.

The calculated axial distribution of the average electron density could be readily merged with the radial profile of electron density from equation (16) to yield the full spatial distribution $n(r, z)$ of the electron density in the plasma column.

**3.1.2. Minimum input power to sustain a discharge.** The plasma column sustained by a surface wave ends when the wave power flux $P(z)$ drops below a given level that depends on the discharge conditions. Therefore, to sustain a SWD, the power flux $P_0$ leaving the launcher must exceed some threshold value such that

$$\min[P_0] = \lim_{z \to l} P(z) \tag{20}$$

where $l$ is the axial position of the end of the column. This means that the plasma column is then extremely short and that its electron density is the lowest for given discharge conditions. This minimum electron density varies in general with the wave dispersion and attenuation, both of which depend on the discharge conditions. As an approximate value for this density, we use $n_D$ as defined in section 2.2.2 for $\nu_{\mathrm{eff}} \ll \omega$.

To estimate the minimum wave power corresponding to the density $n_D$, we return to equation (5) for the power balance in the SWD. Then

$$\min[P_0] \simeq \pi a^2 \theta n_D / 2\alpha(n_D). \tag{21}$$

Note that this relation requires the exact functional dependence $\alpha(\bar{n})$, as calculated from section 2.2.2 and not the approximate relation (13) which diverges at $n = n_D$.

Aside from approximating the column density at the end by $n_D$ (see the footnote to equation (13)), there is at least one additional factor that makes equation (21) an approximation that must be met with some safety margin. That is because equation (5) assumes that all the energy acquired by the electrons at any axial position is lost radially at that same position, while for a very short plasma column, as is the case here, there is a significant increase in the value of $\theta$ caused by the axial loss of charged particles through the extremities of the column.

**3.1.3. The fundamental functions of a surface-wave plasma source.** So far we have concentrated on the various physical processes that determine the ability of the surface wave to establish its own waveguiding structure. We now turn to the functions that must perform any practical set-up for generating efficiently a surface-wave plasma. Figure 8 shows the corresponding essential parts of such a set-up. In this section, we first review briefly the wave launcher functions and then consider them in more detail in sections 3.2 to 3.4.

The field applicator provides the appropriate electromagnetic field distribution in the wave excitation region in order to launch a surface wave in a given

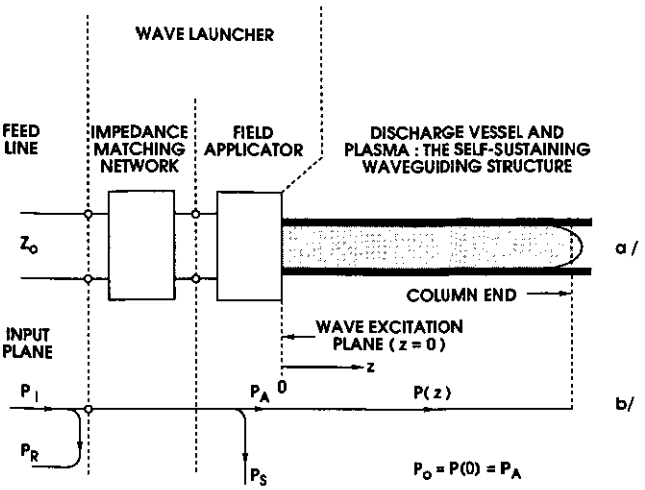


**Figure 8.** Surface-wave plasma source (*a*) and power flow within it (*b*). $P_I$, $P_R$, $P_S$ and $P_A$ denote respectively the power incident in the feed line, that reflected at the launcher input, the radiated power, and the power absorbed in the plasma. $P(z)$ is the axial power flux of the surface wave, decreasing from $P_0$ at the launcher to almost zero at the end of the column.

mode, while the impedance matching network optimizes the power transfer to the plasma. These two components perform the fundamental functions associated with the launching. We shall call the pair the wave launcher (as we shall see, these two parts of a wave launcher cannot always be physically separated). The ideal launcher should accept all of the power coming from the feed line, and fully convert it into surface-wave power flux.

### 3.2. Launching the surface wave

**3.2.1. The initial stage of a surface-wave discharge.** Though the present work is dedicated to steady-state discharges, let us nevertheless consider briefly the initial phase of the discharge. Obviously, when there is no plasma, the surface wave cannot propagate. Therefore, more complex physical processes than those considered so far are involved during this initial stage.

A qualitative picture of the temporal evolution of the surface wave, starting with the initial breakdown and up to the establishment of a fully developed steady-state discharge, is as follows. The initial breakdown takes place in the discharge tube close to the launcher gap. It occurs either spontaneously, when the intensity of the field extending from the launcher is large enough, or it can be triggered by the field of an auxiliary source, e.g. a Tesla coil. Due to the field gradients within the gap region of the exciter, the electrons are driven along the tube axis by the ponderomotive force (Bloyet *et al* 1981). Once the electron density $\bar{n}$ in the launching area exceeds $n_D$, the surface wave propagates until it is reflected back at the axial position where $\bar{n} \approx n_D$. This creates a large axial gradient of electric field at the reflection point, and electrons are ejected forward forming an ionization front that produces an additional segment of plasma column. This process allows the electromagnetic field to gradually extend away from the launcher, the ionization front moving along with the wave field. The discharge build-up goes on until the plasma column is fully developed. The total column length reached in this way depends on the amount of power delivered to the launcher.

For a detailed analysis of the initial stage of surface-wave sustained discharges, and for data concerning their operation under a pulsed regime, see Bloyet *et al* (1981), Llamas *et al* (1985) and Gamero *et al* (1985, 1988).

**3.2.2. Setting a given mode of wave propagation.** In plasma physics, the problem of launching surface waves was first encountered in experiments on the propagation of non-ionizing (i.e. small amplitude) electromagnetic waves (see, for example, reviews by Shivarova and Zhelyazkov 1978 and by Moisan *et al* 1982a).

In the case of non-ionizing waves, the wave mode (section 2.2.1) appears to be fully determined by the field distribution imposed by the field applicator. However, this does not apply to surface waves sustaining a discharge. This problem was studied in detail by Margot-Chaker *et al* (1989) for the $m = 0$ and $m = 1$ modes, and we shall now summarize some of their findings. (i) The $m = 1$ mode wave can be launched to sustain a plasma column only provided that the product of the wave frequency $\omega/2\pi = f$ and tube radius $a$ exceeds some critical value, namely 2 GHz cm. (ii) The $m = 0$ mode wave can propagate and sustain the plasma whatever the value of $fa$, but it is difficult to launch this wave when $fa > 2$ GHz cm. This creates difficulties when striving to sustain plasmas in large diameter tubes using the $m = 0$ wave. Discharge tubes with a tapered transition section can then be used (section 5), with the wave being launched over the small diameter section of the vessel. With enough power at the launcher, the wave extends into the large-diameter section to sustain the plasma.

### 3.3. The efficiency of power transfer from the HF generator to the plasma in surface-wave discharges

When a plasma is generated with surface waves, in contrast to non-ionizing wave propagation experiments, rather high power levels may be involved. The efficiency of the plasma source is then an important parameter. The plasma volume or the plasma density increases with it, whereas the occurrence of power losses in parts of the set-up other than the plasma column can damage components. We define the efficiency as the fraction of the power delivered by the HF generator at the source input that is absorbed into the plasma.

In a surface-wave plasma source, there are three possible loss mechanisms: reflections at the feed line–source interfaces, losses in the dielectric and metallic

elements of the plasma source, and radiation of non-guided waves into the surrounding space. By careful design of the wave launcher the first two types of loss (i.e. those occurring within the field applicator and in the impedance matching network) can be kept small compared with the power absorbed into the plasma. We disregard them here but regular checks should be made when operating a plasma source.

To quantitatively analyse the power transfer process, we use the concepts of coupling and launching efficiency developed in connection with terrestrial surface waves (Barlow and Brown 1962). Refer to the power flow graph in figure 8(*b*) where $P_I$, $P_R$, $P_A$ and $P_S$ denote, respectively, the incident and reflected wave power flux in the feed line, the power absorbed into the plasma and the power lost due to radiation (non-guided wave).

The coupling efficiency depends only on the wave reflection at the feed line–launcher interface and thus

$$\eta_C = (P_I - R_R)/P_I. \tag{22}$$

The launching efficiency is the fraction of the total power leaving the launcher that is converted into surface-wave power flux. This power is considered to be fully† used to sustain the plasma column. Thus, the launching efficiency is

$$\eta_L = P_A/(P_A + P_S) = P_A/(P_I - P_R). \tag{23}$$

The remaining part of the power that leaves the launcher $P_S$ radiates into space in the form of an undesired non-guided wave. It is fortunately possible, as a rule, to keep this radiation at a very low level by a proper design of the launcher and by adequate operating conditions.

The overall efficiency of the surface-wave plasma source is then

$$\eta = \eta_C \eta_L = P_A/P_I. \tag{24}$$

In most practical instances, the amount of power radiated into space is negligible compared with that transferred to the discharge. Then, the coupling efficiency between the feed line and the wave launcher is the single factor determining the overall efficiency of the surface-wave plasma source $\eta$ and

$$\eta = P_A/P_I \simeq (P_I - P_R)/P_I. \tag{25}$$

This efficiency can be measured directly in the power feeding line using, for example, standard reflectometer techniques (Hubert *et al* 1986).

### 3.4. Impedance matching in surface-wave plasma sources

**3.4.1. The equivalent circuit representation.** In the equivalent circuit of the plasma source, the components are directly related to electromagnetic energy storage or dissipation processes. This yields the HF characteristics of the plasma source by circuit analysis rather than by solving the electromagnetic field equations. Looked at from the side of the feed line, the plasma source constitutes a lossy termination.

Optimizing the power transfer from the feed line to the plasma source basically means, according to equation (25), that as little as possible of the wave power should be reflected at the launcher input. In the present case, this can be accomplished by using, ahead of the field applicator (figure 8), a network that can consist either of intrinsic tuning means, i.e. incorporated into the applicator structure, or of physically separated tuning elements. In terms of HF circuit theory (Kerns and Beaty 1967) the surface-wave launcher may be regarded as a 'transducer', i.e. as a device for transferring power from a given mode in a waveguide to a given mode in another waveguide. We now discuss the plasma source equivalent circuit, starting with the gap impedance.

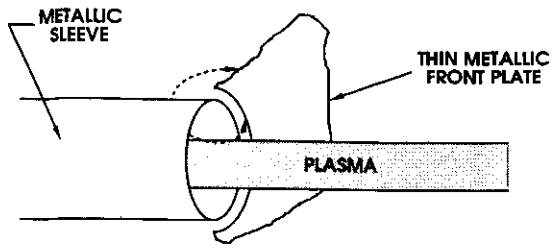


**Figure 9.** Elements forming the field-shaping structure for exciting $m = 0$ mode surface waves. This wave-launching gap consists of a cylindrical metallic tube surrounding the discharge tube (or a dielectric material link to the discharge tube) and, perpendicular to it, a thin metallic plate. With a tight-fitting metallic sleeve around the dielectric tube, the propagation of the wave excited at the gap towards the metallic sleeve is nearly choked. This usually gives rise to a longer plasma column on the other side of the gap, where the discharge tube is surrounded by air. The arrows show electric field lines.

**3.4.2. Gap impedance.** Figure 9 shows the most common type of wave-launching aperture for sustaining a plasma column with a surface wave. This aperture consists of a cylindrical metallic tube, generally surrounding the discharge tube, and a thin metallic plate located perpendicularly to the tube axis and positioned at a few millimetres from it. The launcher establishes in the gap region a large electric field that excites the wave. With a proper design, most of the power leaving the gap is carried away by two oppositely directed surface waves, and this power is gradually used up along the discharge to sustain it. In addition, reactive energy is stored in the electromagnetic field at and in the vicinity of the gap, and a small amount of power is dissipated in the plasma located in the region of the gap. The corresponding equivalent circuit is shown in figure 10. Here, $R_{w1}$ and $R_{w2}$ are the characteristic impedances of the plasma column as seen, respectively, by waves 1 and 2, that propagate in opposite directions

† This is generally true with the $m = 0$ mode but not with higher modes. For example, a significant part of the power flux remains past the column end with the $m = 1$ mode when the product $fa$ is not much larger than 2 GHz cm (Margot-Chaker *et al* 1989).

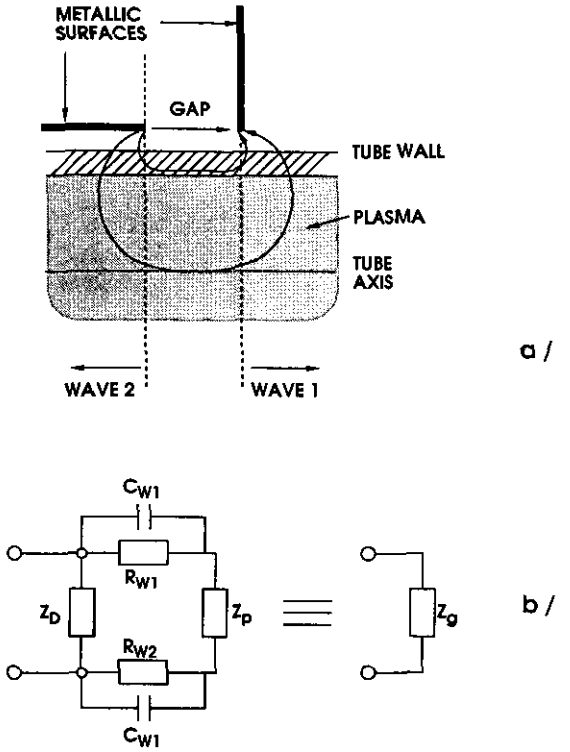


**Figure 10.** Electric field distribution in the gap region where a surface wave is launched in both directions (*a*) and the corresponding equivalent circuit (*b*) representing the wave power transport ($R_w$), the power dissipation (Re($Z_d$) and Re($Z_p$)) and energy storage ($C_w$, Im($Z_D$) and Im($Z_p$)) processes in the gap region. As usual, Re and Im denote the real and imaginary parts of a complex number respectively. The resulting impedance $Z_g$ is called the gap impedance.

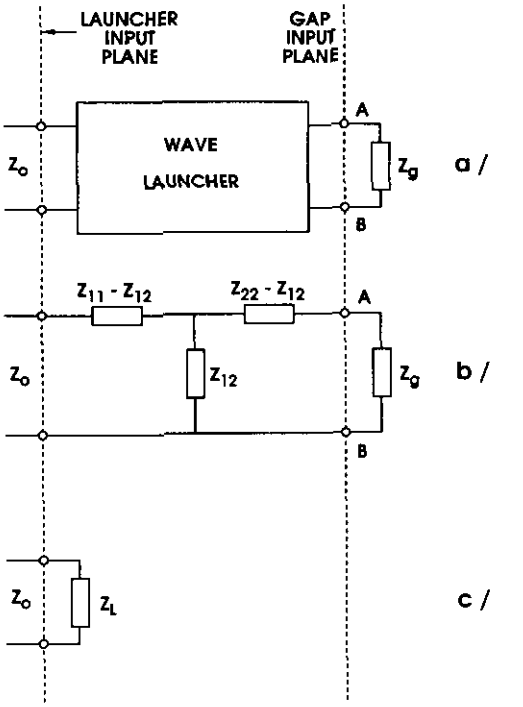


**Figure 11.** The wave-launcher as a two-port network inserted between the feed line of impedance $Z_0$ and the gap impedance $Z_g$ (*a*), its equivalent **T** circuit (*b*), and the equivalent one-port termination $Z_L$ (*c*) representing the plasma–source impedance.

away from the gap. These impedances are connected with the power carried away by the waves, while the capacities $C_w$ take into account the energy storage associated with the wave launching. To account for the energy dissipation and the energy storage in the gap region itself, we use $Z_p$ for what happens within the plasma and $Z_D$ outside it. The resulting impedance $Z_g$ seen at the gap when a surface-wave discharge is sustained (in short, the gap impedance) is defined with respect to a reference plane chosen in the launcher structure.

Since the power losses in the discharge tube walls and within the plasma in the gap region are negligible compared with the wave power flux, all the elements in the equivalent circuit of figure 10, besides $R_w$, can be considered to be imaginary ($Z_p = jX_p$, $Z_D = jX_D$). If the conditions of wave launching in both directions from the gap are approximately the same, a somewhat simplified case results where $R_{w1} \simeq R_{w2} = R_w$ and $C_{w1} \simeq C_{w2} = C_w$. The gap impedance, more easily expressed as an admittance $Y_g$, is then given by

$$\frac{1}{Z_g} = Y_g = G_g + jB_g$$
$$= \frac{1}{R}\frac{1}{1+(X/R)^2} - j\left(\frac{1}{X_D} + \frac{X/R}{1+(X/R)^2}\right) \qquad (26)$$

with $R = 2R_w/(1 + \omega^2\tau_w^2)$ and $X = X_p - 2R_w\,\omega\tau_w/(1 + \omega^2\tau_w^2)$, where $G_g$ and $B_g$ are the gap conductance and susceptance respectively, and $\tau_w = R_wC_w$.

Our representation of the wave launching process by a resistance and a capacitance is consistent with the equivalent circuit proposed by Barlow and Brown (1962) for the terrestrial radio surface-wave launchers.

**3.4.3. Wave launcher impedance.** The wave launcher can be represented (figure 11(*a*)) as a two-port network inserted between the feed line of impedance $Z_0$ and the gap of impedance $Z_g$. Figure 11(*b*) shows one of the possible equivalent circuits for the launcher. This is the **T**-circuit impedance configuration. In the customary notation, $Z_{11}$ is the input impedance of the network with an open output and $Z_{22}$ is the corresponding impedance in the inverse situation. Since we have neglected the energy loss within the launcher, the equivalent network is lossless and all impedances are imaginary: $Z_{11} = jX_{11}$, $Z_{22} = jX_{22}$, $Z_{12} = jX_{12}$. In figure 11(*b*) the wave launcher is represented as an entity. If the field shaping structure and the impedance-matching network are separate units as in figure 8, we obtain tandem (cascade) networks, that can readily be transformed into a single network.

**3.4.4. Impedance matching for minimum reflection or for maximum power transfer.** The total input impedance $Z_L$ (figure 11(*c*)) is the load impedance presented to the feed line by the plasma source. To relate this

impedance to the efficiency of the power transfer, we turn to standard methods of transmission line analysis.

The quantity that characterizes both the impedance mismatch of a transmission line and the wave reflection level within it is the reflection coefficient

$$\Gamma_L = \frac{Z_L - Z_0}{Z_L + Z_0} = \frac{z_L - 1}{z_L + 1}. \tag{27}$$

The lower-case letters denote the impedances normalized with respect to $Z_0$, which is a real quantity, and we have

$$z \equiv Z/Z_0 \equiv R/Z_0 + jX/Z_0 \equiv r + jx. \tag{28}$$

The squared absolute value of the reflection coefficient is equal to the fraction of the incident wave power that is reflected at the launcher input

$$|\Gamma_L|^2 = P_R/P_I. \tag{29}$$

Considering that there are no losses within the launcher and no radiation into space, the overall efficiency of the launcher follows from equations (25) and (29):

$$\eta \simeq 1 - |\Gamma_L|^2. \tag{30}$$

We are now ready to discuss the conditions for impedance matching in the plasma source. A variable load impedance will absorb the maximum possible power from the generator when it is equal to the complex conjugate of the output impedance of the generator: this is conjugate impedance matching. On the other hand, there is no reflected wave in the feed line only when $\Gamma_L = 0$. The latter condition calls for the termination of the feed line with an impedance equal to $Z_0$: this is image impedance matching. Therefore, in general, one faces a dilemma: one can either maximize the power delivered to the plasma or avoid the undesired effects associated with the presence of a reflected wave in the feed line, namely increased power loss along the feed line and possible unstable operation of the plasma source (Hubert *et al* 1986). This dilemma is usually resolved in favour of the image impedance matching, since two factors tip the scale: the tuning for $\Gamma_L = 0$ is easy to monitor and in most practical plasma sources, a circulator (whose input and output impedances are equal to $Z_0$) is inserted between the generator and the launcher input mainly to avoid unstable operation. With this configuration, the generator is always terminated with $Z_0$ and the impedance seen from the launcher input toward the generator also equals $Z_0$. Then only the impedance matching on an image–impedance basis is possible, requiring tuning for minimum $P_R$. The corresponding perfect match conditions at the launcher input are

$$\begin{aligned} &R_L = Z_0 \qquad X_L = 0 \\ \text{or} \\ &r_L = 1 \qquad x_L = 0. \end{aligned} \tag{31}$$

To fulfil the above conditions, at least two of the reactances in the equivalent circuit of the plasma source must be variable. In practical terms, the source has to be equipped with at least two independent tuning means.

## 4. Efficient surface-wave launchers for plasma sources

The wave launcher constitutes the core of any travelling-wave plasma source. The development of efficient, easy to make, and convenient to use wave launchers was a key factor for the progress in SWD research and applications, rendering them competitive with other HF plasma sources.

### 4.1. A family of $m = 0$ mode surface-wave launchers

Various devices, some of them quite ingenious, have been used for launching non-ionizing surface waves (for a review see Moisan *et al* (1982a)). These devices are, in general, of limited use as plasma sources because they are intended for low-power operation, and hence lack overall energy efficiency and power handling capability. This has led us, over the last several years, to develop various $m = 0$ surface-wave plasma sources that comply with the requirements formulated in section 3. This paper presents for the first time a unified discussion of these devices, which are shown in figure 12. Some of their design features, together with their operating frequency range, are listed in table 1. We distinguish between two kinds of launcher: the modular design in which the field-shaping and impedance-matching functions are performed by separate modules, and the integrated design where a single structure performs all the launcher functions.

In all these launchers, the field shaping function is achieved by a circular gap (figure 9) that provides an azimuthally symmetric field distribution similar to that of the $m = 0$ mode wave. The efficiency of the power transfer is obtained by different tuning means for each of these launchers. At the lowest frequencies, our matching networks consist of lumped elements in the form of coils and capacitors. With increasing frequency, we use distributed reactances†, first in the form of coaxial elements and then as waveguide elements.

The family, as a whole, ensures the efficient transfer of HF power from the generator to the plasma in complementary frequency domains over a range extending from approximately 1 MHz to 10 GHz. We have demonstrated the possibility of sustaining surface-wave plasmas at much lower frequencies, namely at 200 kHz (Ricard *et al* 1988), but so far at lower efficiencies. It is thus possible to choose an appropriate launcher at the frequency needed to match available HF generators or at that required to optimize the properties of the plasma produced (Moisan *et al* 1991).

† At frequencies of hundreds of MHz and higher, pure inductance $L$ or capacitance $C$ usually cannot be realized in the form of lumped elements since their dimensions become comparable to the wavelength.

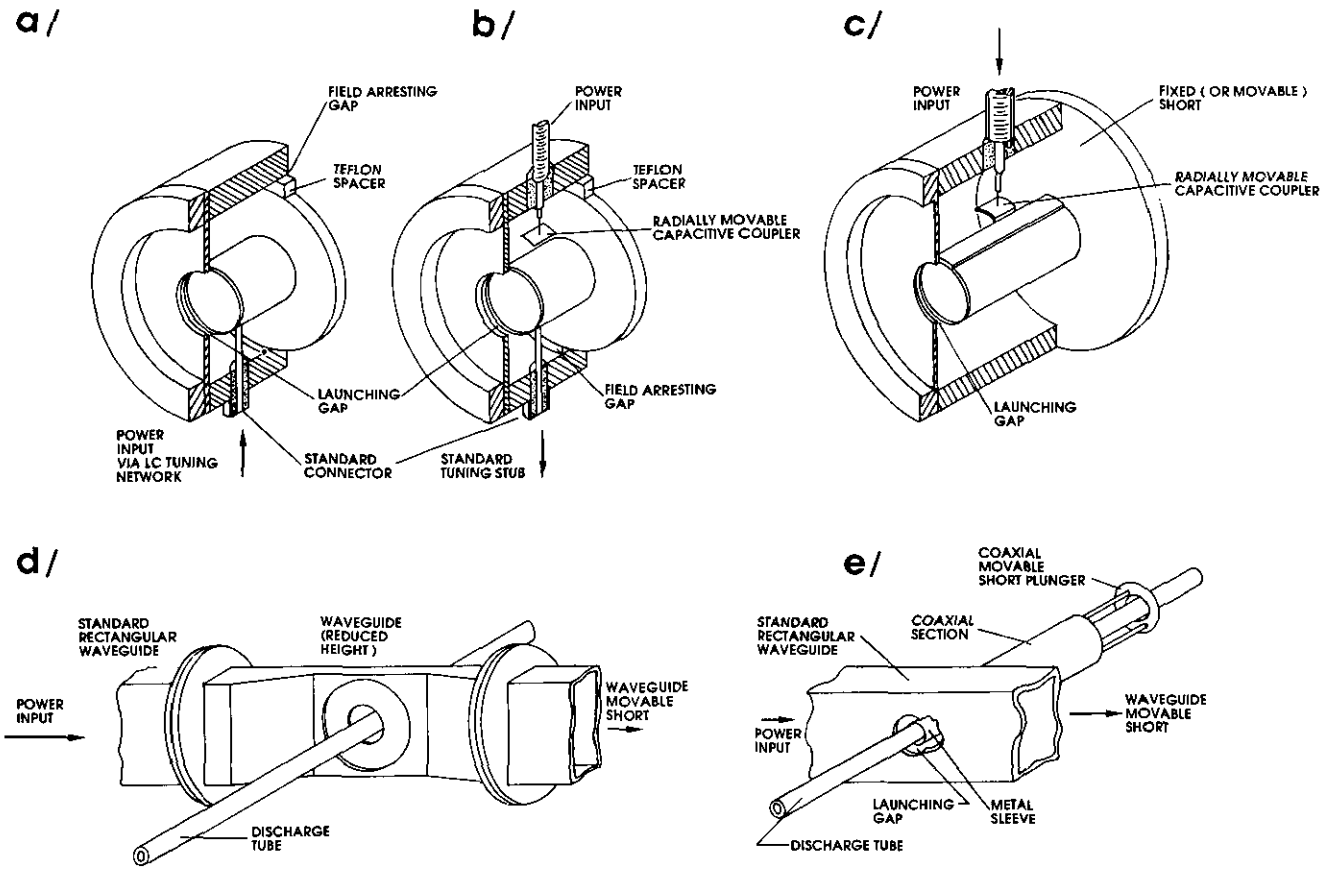


**Figure 12.** A family of $m = 0$ mode surface-wave launchers: (*a*) The Ro-box field applicator to be used with an LC impedance-matching network, (*b*) the Ro-box field applicator with a capacitive coupling to the feeder, to be used with a stub tuner, (*c*) the surfatron, (*d*) the surfaguide field applicator, (*e*) the waveguide–surfatron, without the waveguide movable short-circuit.

**Table 1.** Designation and distinguishing features of efficient surface wave launchers for plasma generation.

| Name | Design | HF feeder | Frequency range (Hz) $10^5$ $10^6$ $10^7$ $10^8$ $10^9$ $10^{10}$ |
|---|---|---|---|
| Ro-box (LC) | Modular[a] | Coaxial | |
| Ro-box (stub) | Modular | Coaxial | |
| Surfatron | Integrated[b] | Coaxial | |
| Waveguide–surfatron | Integrated | Waveguide | |
| Surfaceguide | Modular[a] | Waveguide | |

[a] A modular device is made from separated, interchangeable field shaping and impedance matching units.
[b] An integrated device performs both field shaping and impedance matching functions.
▬ Frequency range corresponding to zero reflected power.

The power handling capability depends mainly on the design of the launcher. With the lumped element network or with the coaxial structures that have been tested to date, it amounts to approximately 1 kW in the RF range (≤300 MHz). With devices using coaxial cables, because dielectric losses increase with frequency, the power is limited to about 400 W at 2450 MHz. The waveguide-based structures allow larger power levels: for example, we have operated an 8 GHz waveguide–surfatron at up to 5 kW.

The members of the launcher family shown in figure 12 have been described previously in scientific journals. We now review them, not in the order of their development, but according to an increasing frequency of operation, a parameter that strongly reflects the design of the launcher. We thus start with the device that uses lumped LC elements, and then pass on to launchers supplied directly from a coaxial line, and, finally, to those based on a waveguide.

### 4.2. The LC Ro-box

The Ro-box field applicator used with an LC impedance matching network, called the LC Ro-box launcher

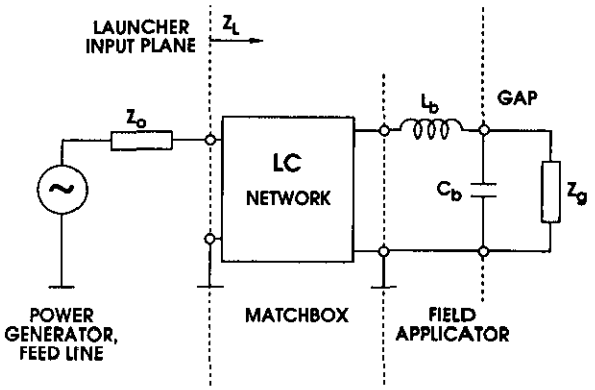


**Figure 13.** Equivalent circuit of the plasma source using the LC Ro-box. $Z_L$ is the impedance seen at the launcher input. The field applicator is represented by the inductance $L_b$ and the capacitance $C_b$. The latter is related to the energy stored in the electric field within the applicator when it is not loaded with plasma.

(Moisan and Zakrzewski 1987, 1988, 1989), operates in the lowest frequency domain (approximately 1–100 MHz) of all the sources listed in table 1. It consists of two separate units: the field applicator (or field shaping) module and a matchbox, an impedance matching network containing LC elements.

The field applicator may be considered as a coaxial line terminated at each end by a capacitive interstice or gap. The outer and inner coaxial metallic cylinders constituting this line are respectively attached to the front and back plate of the applicator, as in figure 12(*a*), forming a launching gap and a field arresting gap. The former opens on the wall of the discharge tube for the field coming out from the Ro-box to penetrate into the plasma. The front plate of the Ro-box must be made as thin† as possible, so as not to obstruct the wave propagation. The other interstice, called the rear or field arresting gap, is required because the back plate and the outer metallic cylinder of the Ro-box must not be in contact in order to achieve a high intensity field at the launching gap‡. However, if the opening made for that purpose at the back of the Ro-box is large, the field coming out there will interfere with that from the surface wave excited at the launching gap and propagating towards the back of the launching gap. Thus, the width of this gap must be small enough, and located radially as far away as possible from the discharge tube, to reduce significantly the field leakage outside toward the discharge tube, but not too small to lead to HF arcing.

The HF power is supplied to the field applicator via a matchbox. This two-port network is inserted between the applicator and the feed line. Figure 13 shows an equivalent circuit for the plasma source using a LC Ro-box. The field applicator is represented by a simple

† This remark applies to all other launchers presented here: typical thickness 0.2–0.5 mm.

‡ At higher frequencies, such a high intensity field can be obtained even though there is no rear gap, provided that the length of the inner coaxial line of the launcher is approximately $\lambda_0/4$.

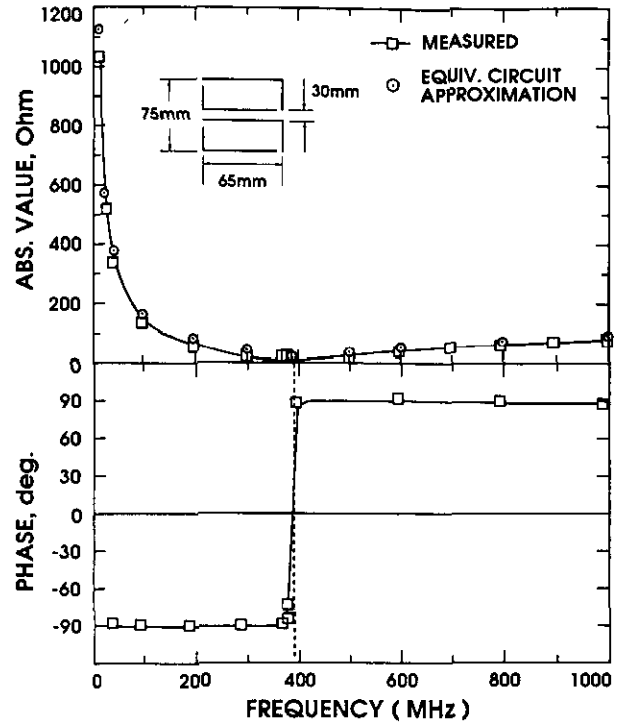


**Figure 14.** Input impedance $Z_b = |Z_b| e^{j\zeta}$ of a Ro-box field applicator, without a plasma column within the gap, against frequency. The inset shows the approximate dimensions of the applicator tested.

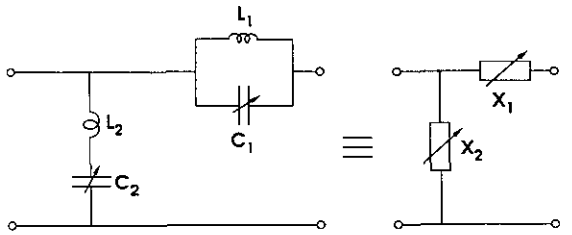


**Figure 15.** Equivalent circuit of one possible matchbox configuration for an LC Ro-box plasma source.

network composed of an inductance $L_b$, related mainly to the existence of the connecting wire within the coaxial structure, and a capacitance $C_b$, which is connected to the energy stored in the electric field within the structure, when it is not loaded with the plasma. To test the validity of this representation for the present field applicator, we measured the total complex impedance $Z_b \exp(j\zeta)$ at the input of such an unloaded field applicator as a function of frequency. A typical result is shown in figure 14. The impedance

$$Z_b = j[\omega L_b - (\omega C_b)^{-1}] \qquad (32)$$

obtained from the equivalent circuit representation, where $L_b$ and $C_b$ are determined from the best fit to the measured data, agrees well with the experimental data.

An efficient matchbox can be made using, for example, the simple network shown in figure 15

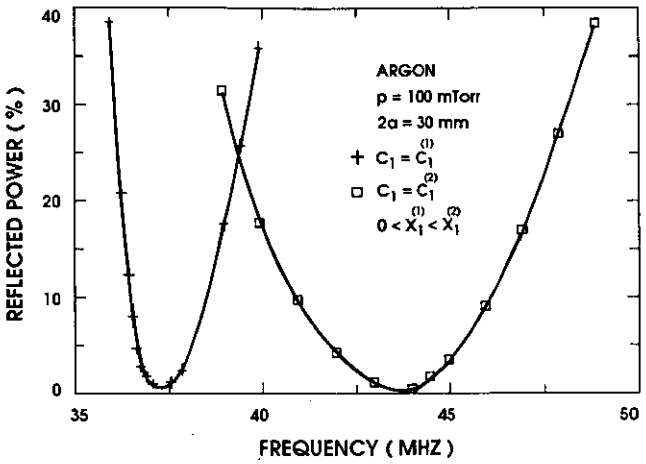


**Figure 16.** Observed frequency characteristics for an LC Ro-box plasma source employing the matchbox of figure 15 and the field applicator of figure 14, under fixed discharge conditions and for constant incident HF power to the launcher. The value of $X_1$ (figure 15) is set through $C_1$ and then remains fixed for a given curve, while the value of $X_2$ is adjusted at each frequency for minimum reflected power.

(Moisan and Zakrzewski 1987). For that circuit, the matching conditions are

$$1/x_1 = b'_g \pm (g_g - g_g^2)^{1/2} \tag{33}$$

$$x_2 = \mp (1/g_g - 1)^{1/2} \tag{34}$$

where $x_1 = X_1/Z_0$ and $x_2 = X_2/Z_0$ are the normalized reactances of each tuning element, $Z_0/Z_g = g_g + jb_g$ is the normalized input admittance of the gap when sustaining a discharge, and $b'_g = b_g + j\omega C_b$, assuming that the influence of $L_b$ is negligible at low frequencies. Numerous other forms of matching network are possible. For example, one may find that using the circuit of figure 15, but with interchanged input and output ports, facilitates matching.

To illustrate the tuning process, we measured the power reflected at the input of the launcher as a function of the wave frequency, as shown in figure 16. The two curves were obtained under the same discharge conditions and for a constant level of incident HF power to the launcher. Each curve corresponds to a fixed value of $X_1$ in figure 15, while the value of $X_2$ at each frequency is adjusted for minimum reflected power. We observe that: (1) for a given value of $X_1$, there exists one frequency at which the system can be perfectly matched; (2) the lower the frequency of operation, i.e. the frequency at which one wants to obtain zero reflected power, the sharper is the tuning process.

The frequency range for efficient operation of this source extends from approximately 1 MHz, the lowest value of our present family of surface-wave plasma sources, up to over 100 MHz. The maximum input power to the applicator depends mainly on the quality of the coaxial cables and connectors. As for the LC matchbox, it can be made to withstand large power levels but at the cost of large dimensions. The practical power handling capability of the LC Ro box is of the order of 1 kW. This limit could be raised to many kilowatts and the matchbox kept to an acceptable size by using vacuum sealed capacitors and water-cooled coils.

The compactness of the field applicator, even at the lowest frequency of operation, and the versatility that results from the modular design are important features of this launcher. For example, this compact applicator could be situated over a plasma vessel, even if it is inaccessible during operation, and connected by cable to a remote matchbox. Also, a given field applicator module can be used with various matchboxes and vice versa.

### 4.3. The stub Ro-box

This wave launcher uses the same field applicator as that of the LC Ro-box, but its power feed and impedance matching are different. The HF power is supplied to the launcher via a coaxial feed line through a capacitive coupler (figure 12(*b*)). This impedance tuning element is constructed from a section of semi-rigid cable that penetrates radially into the field applicator module. The extremity of the cable extending outside the Ro-box is terminated by a standard coaxial line connector. The outer conductor at the extremity of the cable within the structure is removed over 5 to 10 mm and a thin metal plate, typically 10 mm × 10 mm, attached transversely at the end of the inner conductor. This assembly is moveable in the radial direction with no possibility of rotation, and its electrical connection with the structure wall is assured by flexible finger-type contacts. This coupler provides a variable capacitance $C_c$ and an inductance $L_c$ between the inner tube of the field applicator and the feed line.

The second tuning adjustment is a standard coaxial stub, i.e. a variable length $l_s$ of coaxial line terminated by a short-circuit. This stub is connected to the second port of the Ro-box applicator, as in figure 12(*b*), and is the origin of the name stub Ro-box given to this launcher (Moisan and Zakrzewski 1987, 1988, 1989). The capacitive coupler and the variable-length stub provide adequate tuning to optimize the power transfer to the plasma, as we shall now see.

Figure 17 shows the equivalent circuit of the plasma source using a stub Ro-box. In this and in the following equivalent circuits the distributed elements are shown as bold lines. The input impedance of the launcher normalized with respect to $Z_0$ is

$$\frac{Z_L}{Z_0} \equiv \frac{R_L}{Z_0} + \frac{jX_L}{Z_0} = \frac{g_2}{g_2^2 + (b_2 - b_1)^2} + j\left(\frac{\omega L_c}{Z_0} - \frac{1}{\omega C_0 Z_0} - \frac{b_2 - b_1}{g_2^2 + (b_2 - b_1)^2}\right) \tag{35}$$

where

$$b_1 = Z_0[\omega L_b + Z_{os} \tan(2\pi l_s/\lambda_0)]^{-1}$$

$$g_2 = g_g = Z_0 G_g$$

$$b_2 = Z_0(\omega C_b + B_g).$$

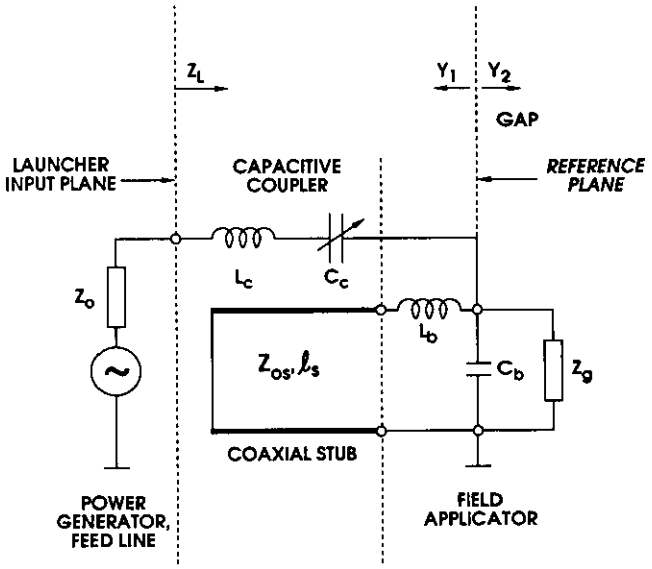


**Figure 17.** Equivalent circuit of the plasma source using the stub Ro box. Bold lines represent distributed elements.

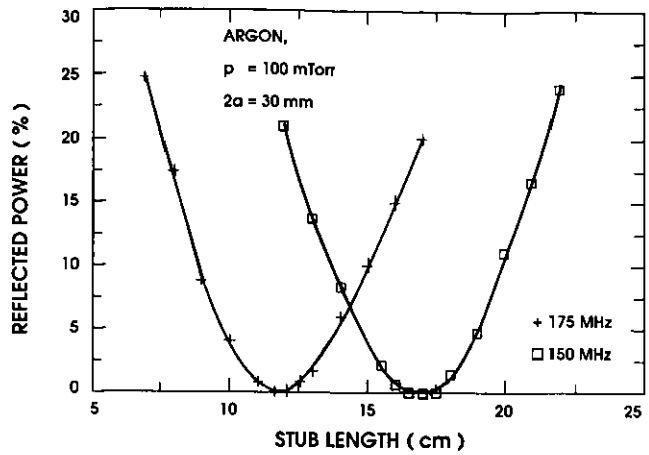


**Figure 18.** Observed tuning characteristics of a stub Ro box operated at two frequencies, the other discharge conditions being fixed. The stub length is measured from its connecting port on the Ro box. The field applicator is the same as in figure 14 (inset).

Here $Z_{os}$ is the characteristic impedance of the stub coaxial line and $G_g + jB_g \equiv Z_g^{-1}$ is the gap admittance (section 3.4.2). As shown in figure 17, $y_1 = Z_0 Y_1 \equiv -jb_1$ and $y_2 = Z_0 Y_2 \equiv g_2 + jb_2$ are normalized admittances seen in each direction from the reference plane which coincides with the coupler axis. The admittance $Y_1$ is imaginary for a lossless structure.

Applying the general impedance-matching conditions of equation (31) for the resistance and the reactance at the launcher input to the case of a stub Ro-box plasma source one obtains

$$(b_2 - b_1)^2 = g_2 - g_2^2 \tag{36}$$

and

$$\omega L_c - \frac{1}{\omega C_c Z_0} = \pm \left(\frac{1}{g_2} - 1\right)^{1/2}. \tag{37}$$

Under given discharge conditions and for a given field applicator the only two parameters affected by the tuning are $C_c$ and $b_1$. The value of $C_c$, which affects only the imaginary part of $Z_L$, varies with the radial position of the coupler while $b_1$ depends on the stub length $l_s$.

As can readily be seen from the last two equations, it is only when $g_2 \leqslant 1$, i.e. $G_g \leqslant Z_0$, that the matching conditions (36) and (37) can be met for full power transfer to the plasma. Figure 18 shows the tuning characteristic† of the stub Ro-box at two operating frequencies.

Compactness and versatility are strong features of the stub Ro-box and the tuning is, in most instances, a simpler procedure than with the LC Ro-box. In practice, the frequency range over which a perfect match can be achieved is approximately 150–1000 MHz‡. The power handling capability is mainly determined by the quality of the cables and connectors, as well as by the tuning stub design.

### 4.4. The surfatron

Historically, the surfatron (Moisan *et al* 1974, 1975, 1976, 1977) was the first surface-wave launcher of the present family to be developed. Also, it is the one that has found the widest recognition and use as a source of long plasma columns for physical studies, plasma chemistry, plasma processing, and laser engineering. In fact, the term 'surfatron plasma' is used by some authors to designate surface-wave sustained plasmas.

The surfatron, shown in figure 12(*c*), is an integrated wave launcher that performs both field shaping and impedance matching. The field shaping is provided by the same circular gap as in a Ro-box. The external stub used in the stub Ro-box launcher is now part of the surfatron body: the coaxial structure extending to the back of the surfatron, past the coupler's plane, is a coaxial line terminated by a short-circuit. This short circuit is movable for broadband operation.

Figure 19 shows the equivalent circuit of the surfatron. Notice that it is the same as that of the stub Ro-box, except for two minor changes: in the case of the surfatron $L_b = 0$ and we added a transmission line of characteristic impedance $Z_{os}$ and length $l_2$. However, the input impedance and the impedance-matching conditions are the same as in equations (35) to (37), the quantities $b_1$ and $Y_2$ being defined slightly differently: since $L_b = 0$, the corresponding term in $b_1$ vanishes; the value of $Y_2$ is now the gap admittance as seen in the reference plane, i.e. once it has been transformed along the transmission line of characteristic impedance $Z_{os}$ and length $l_2$. The influence of this short-line

† Henceforth, we shall refer to the tuning characteristic as the dependence of $P_R/P_I$ on the axial length of the adjustable short-circuit, with the other tuning element of the launcher set for minimum reflection.

‡ Stub Ro-boxes with discharge tube diameters smaller than 10 mm have been operated at 2.45 GHz, but it seems that losses in the stub are larger than with a surfatron.

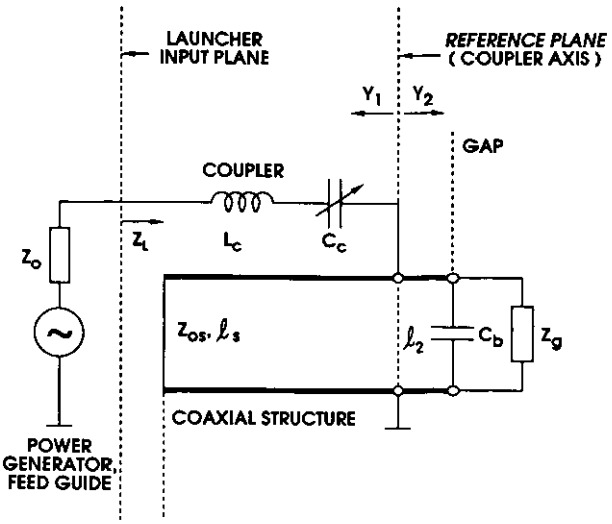


**Figure 19.** Equivalent circuit of the surfatron plasma source.

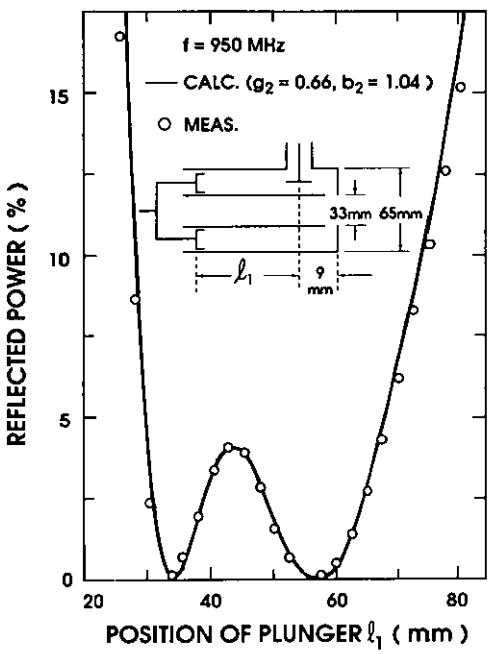


**Figure 20.** Measured and calculated tuning characteristics of the surfatron. The theoretical curve is obtained from the equivalent circuit where the values of $g_2$ and $b_2$ have been calculated from the two $l_1$ positions where there is zero reflected power (Moisan *et al* 1979a, b). The insert shows the approximate dimensions of the launcher parts.

impedance transformation increases with increasing frequency and it may be instrumental in determining the upper frequency of operation of the surfatron (Moisan *et al* 1979a).

The tuning procedure of the surfatron, in principle, is the same as for the stub Ro-box since the difference between these two launchers is only structural, as already mentioned. In what follows, we discuss the tuning characteristic of the surfatron in more detail. Figure 20 shows such a typical tuning characteristic. The values of $P_R/P_I$ calculated from the above formulae are compared with the measured values. The calculated curves were fitted to the experimental results at the two $l_1$ positions corresponding to zero reflected power. In this procedure, we implicitly assume that the plasma column parameters do not vary during the tuning process. This is not necessarily the case since these curves have been obtained not at a constant absorbed power, but at a fixed incident HF power. Experimentally, the procedure is found to be satisfactory, provided that the reflected power at the launcher input remains less than approximately 30%. Under these operating conditions, and with the surfatron's coupler always tuned for the minimum reflected power, $g_2$ and $b_2$ are found to be constant and the power transfer into the plasma thus depends only on the plunger position, as can be seen from the good agreement between the calculated and the measured values in figure 20. For more details on the modelling of the surfatron and its experimental verification, as well as for operating data, see Moisan *et al* (1979a).

There is no lower limit to the working frequency of a surfatron coming from its principle of operation. It rather results from practical considerations, namely the size and the weight of the structure, that make it cumbersome at lower frequencies. For example, the total length $(l_1 + l_2)$ of a surfatron working at 100 MHz exceeds 50 cm, this length reaching approximately 4 to 5 m at 13.56 MHz. The upper frequency limit of operation depends on the design of the gap–coupler part of the surfatron (Moisan *et al* 1979a) and decreases with increasing plasma tube radius. The tuning become difficult because of the appearance of higher order coaxial line modes within the structure and of the excitation of surface waves in $m \geq 1$ modes (Margot-Chaker *et al* 1989). With tubes of diameters smaller than approximately 10 mm, surfatrons can be tuned for zero reflected power up to 2.5 GHz. In practice, 2.45 GHz seems to be the maximum frequency for efficient operation of the surfatron.

The power handling capability of a surfatron is limited by the fact that the HF energy is delivered via a capacitive coupler made from a coaxial feed line. The maximum input power is determined mainly by the quality of the cable and connector, and decreases with increasing frequency (Hubert *et al* 1986). From our experience, 500 W CW is really an upper limit for the power of a surfatron at 2450 MHz.

### 4.5. The surfaguide

The limitations in the power handling capability of the surfatron may be overcome and the frequency of operation of the wave launchers increased, by turning to waveguide-based structures. One such device, termed a surfaguide, has been proposed by Moisan *et al* (1976, 1977, 1984) and described in detail in the last of these papers.

The surfaguide is by far the simplest of the surface-wave launchers reviewed here. It consists of two parts:

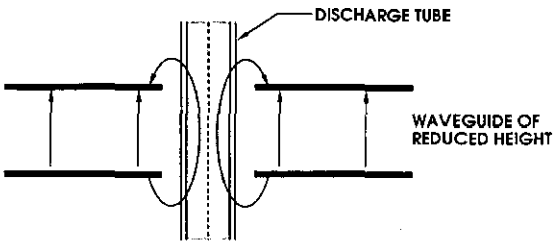


**Figure 21.** A rectangular waveguide with circular holes through the wide walls provides a launching gap where the electric field closely resembles that of figure 9. The waveguide height is much smaller than the surface-wave wavelength.

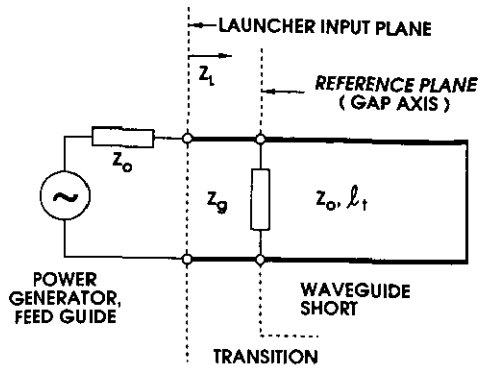


**Figure 22.** Equivalent circuit of the surfaguide plasma source.

(1) a field applicator, as in figure 12(*d*), which is a section of rectangular waveguide of reduced height, tapered symmetrically with respect to the launching aperture; (2) an adjustable waveguide short-circuit (movable plunger) located at one end of the applicator waveguide line. At the opposite end, the microwave power is supplied to the launcher directly from the feed guide. In practice, it is most suitable to base the design of such a launcher on a standard rectangular waveguide, chosen according to the frequency of operation. This permits the use of standard waveguide components for the feed guide, the adjustable short-circuit, and the power monitoring.

To form the wave-launching aperture of figure 12(*d*), a circular hole is pierced through both sides of the wide wall of a lowered-height† waveguide. Figure 21 shows, in a plane parallel to the waveguide small width walls and containing the discharge tube, the approximate electric field orientation of the fundamental $TE_{10}$ mode inside the waveguide, and the field imposed on the discharge in the wave-excitation region. The latter field orientation is essentially the same as the one within the launching gap of the coaxial field applicators already discussed. As for the azimuthal uniformity of the electric field strength recall that, in the transverse cross section of a rectangular waveguide, the electric field of the fundamental $TE_{10}$ mode is uniform in the direction parallel to the narrow walls, but increases as a cosine function from the wall to the axis in the direction parallel to the wide wall. Thus, to maintain an approximately uniform field over the aperture requires a small ratio of the aperture diameter to the guide width. A practical limit is reached when the diameter of the aperture exceeds one quarter of the guide width. This means, for example, that at 2.45 GHz (the frequency most commonly used for sustaining microwave induced plasmas) one can use tubes up to 25 mm in diameter if the applicators are based on the WR-430 standard rectangular waveguide (width 109 mm).

Figure 22 shows an equivalent circuit of the plasma source using a surfaguide. We have represented the energy storage and the power flow processes related to the wave launching by a single impedance $Z_g$ shunting the waveguide at the plane of reference which goes through the gap axis. The impedance associated with the plunger is referred to the same plane. Here, the input impedance $Z_L$ of the source is the impedance at some chosen input plane along the full waveguide. It results from a smooth transformation through the tapered transition of the impedance seen at the reference plane.

Because of the form of the equivalent circuit, it is convenient to discuss the tuning process in terms of the input admittance $Y_L = Z_L^{-1}$, which may be written in a normalized form

$$y_L = Z_0/Z_L \equiv g_L + jb_L = g_g + j(b_g - x_t^{-1}) \quad (38)$$

where $y_g = Z_0/Z_g \equiv g_g + jb_g$ is the normalized gap admittance and $x_t = \tan(2\pi l_t/\lambda_g)$ is the normalized reactance of the movable waveguide plunger. This plunger operates at the fundamental mode wavelength $\lambda_g$ and is terminated by a movable reflecting plane located at a distance $l_t$ from the reference plane. From equations (27) and (29) one obtains

$$\frac{P_R}{P_I} = \left|\frac{1 - y_L}{1 + y_L}\right|^2. \quad (39)$$

The surfaguide has only one readily adjustable component. This means that zero reflected power cannot be achieved under broad operational conditions. Although a minimum for $P_R/P_I$ (corresponding to $b_L = 0$) can always be reached by properly setting the movable plunger, the value of $g_L = g_2$ is fixed, for given launcher and discharge conditions. Nevertheless, as a rule, efficient coupling, say, less than 10% reflected power, can be achieved by optimizing the height of the waveguide in the aperture section, according to the recommendations given by Moisan *et al* (1984).

† The small waveguide height provides a gap width that is much smaller than the wavelength of the wave to be launched. In order to minimize perturbations to the surface-wave field, the diameter of the discharge tube holes through the waveguide is typically 1.2–2 times the outside diameter of the plasma tube, and the wide walls are thinned down to 0.3–0.5 mm around the aperture holes over a radius that is approximately five times that of the tube (see Moisan *et al* (1984) for more detail). The tapered transitions on both sides of the aperture ensure a smooth impedance transformation to the standard waveguide part of the applicator.

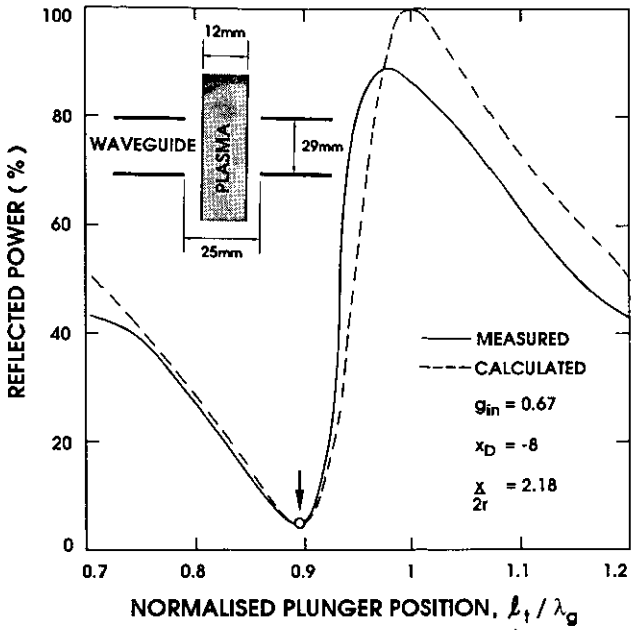


**Figure 23.** Measured and calculated tuning characteristic of a surfaguide plasma source at 2.45 GHz based on a WR-284 waveguide whose fundamental mode wavelength is $\lambda_g$. The arrow shows the plunger position where the calculated curve was fitted.

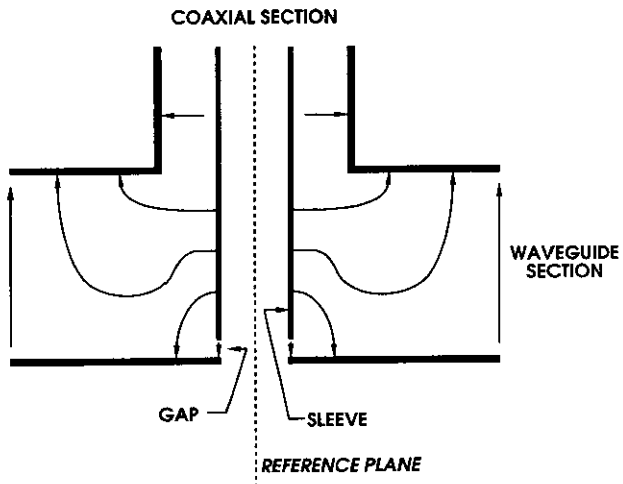


**Figure 24.** The launching interstice or gap in a waveguide–surfatron and the approximate distribution of the electric field in the region adjacent to the reference plane.

Figure 23 shows a comparison between measured and calculated tuning characteristics. The results derived from the simple equivalent circuit presented above are in good agreement with the measured values, except in the region of large reflected power. This discrepancy comes from the influence of the tuning process on the absorbed power, as already mentioned when discussing the tuning characteristics of the surfatron.

With the simple launcher just described, one can obtain satisfactory power transfer to the plasma over a relatively wide range of gas pressure and microwave power. The lower frequency limit of the surfaguide, using standard waveguides and authorized frequencies for industrial, scientific and medical purposes, is 915 MHz. The upper limit is approximately 10 GHz because of the small waveguide dimensions compared with the discharge tube diameters. The power handling capability of such a plasma source is, in practice, determined only by the discharge tube resistance to heating and thermal shocks.

### 4.6. The waveguide–surfatron

The waveguide–surfatron is a surface-wave launcher consisting of both waveguide and coaxial line elements as shown in figure 12(*e*). The microwave power is supplied by the generator to a rectangular waveguide section, terminated, past the launching aperture, by a waveguide with a movable short circuit. An air insulated coaxial line section is attached perpendicularly to the wide wall of the waveguide, and its inner conductor extends into the waveguide, as a sleeve around the discharge tube, forming a circular launching gap in the immediate vicinity of the opposite wall (figure 24). The other end of this coaxial line is terminated by a coaxial movable short circuit. In contrast to the surfaguide it is the gap width not the aperture diameter which determines the field emergence from the waveguide. This permits the excitation of surface waves over discharge tube diameters that approach the guide width.

The waveguide–surfatron features the excellent tuning capabilities of the surfatron and additionally has the high-power handling capability of the surfaguide. Its practical frequency range is the same as for a surfaguide, but it can achieve efficient power transfer to plasma over a wider range of discharge conditions. However, it is mechanically more sophisticated than either the surfatron or the surfaguide, and thus more costly.

The design of the waveguide–surfatron was first disclosed by Chaker *et al* (1982); its theoretical model was proposed and verified experimentally by Moisan *et al* (1987). When the outer diameter of the coaxial section is small compared with the width of the waveguide, the model is simple: all the impedances in the equivalent circuit are related to a single reference plane coincident with the axis of the coaxial section. This reference plane is shown in figure 24, together with a sketch of the electric field distribution in the region adjacent to it. Figure 25 shows the corresponding equivalent circuit. The two distributed elements (bold lines) represent the coaxial and the waveguide adjustable short circuits. The gap impedance when sustaining a plasma is $Z_g$; $Z_s$ accounts for the metal sleeve across the waveguide.

The input impedance $Z_L$ of the waveguide–surfatron is the impedance seen in the reference plane, or in any plane towards the generator, provided that it is located at a distance $k\lambda_g/2$ from the reference plane, where $k$ is an integer and $\lambda_g$ is the wavelength in the

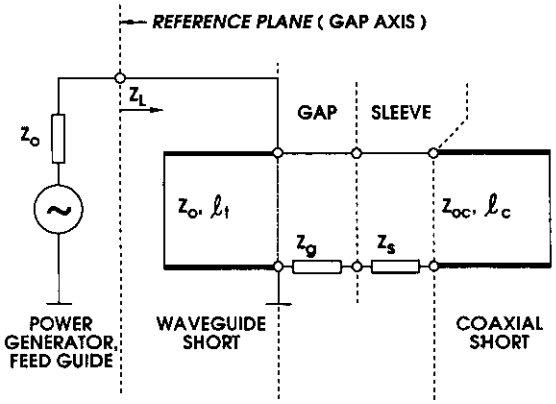


**Figure 25.** Equivalent circuit of the plasma source using the waveguide–surfatron. The characteristic impedances of the waveguide and coaxial lines are $Z_0$ and $Z_{oc}$ respectively. The waveguide and coaxial plunger axial positions are $l_t$ and $l_c$ respectively.

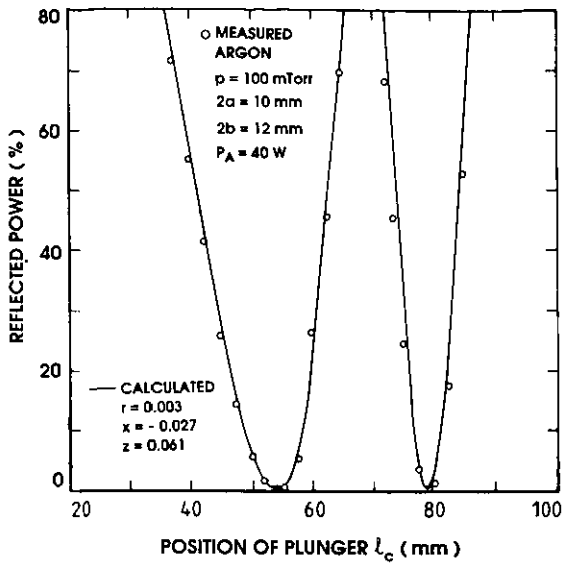


**Figure 26.** Measured and calculated tuning characteristic of the waveguide–surfatron at 2.45 GHz when the outer diameter of the coaxial section is small compared with the width of the waveguide. Here, in contrast to figures 20 and 23, the absorbed power $P_A$, and not the incident power $P_I$, is kept constant. See the text for the launcher dimensions (from Moisan *et al* 1987).

guide. The corresponding normalized admittance can be written as

$$y_L = \frac{Z_0}{Z_L} = g_L + jb_L = \frac{r}{r^2 + (x + x_c)^2} - j\left(\frac{1}{x_t} + \frac{x + x_c}{r^2 + (x + x_c)^2}\right) \tag{40}$$

with

$$x_c = z\tan(2\pi l_c/\lambda_0) \qquad x_t = \tan(2\pi l_t/\lambda_g)$$

where $l_c$ and $l_t$ are the coaxial and waveguide plunger distances respectively, with respect to the reference plane. In our usual notation

$$z_g = Z_g/Z_0 \equiv r_g + jx_g \qquad z_s = Z_s/Z_0 \equiv jx_s$$

and $z = Z_{oc}/Z_c$. Here, $r = r_g$ and $x = x_s + x_g$.

Observe that equation (40) and the corresponding equation for the stub Ro-box (equation (35)) and the surfatron are exact counterparts, with the impedance terms replaced by admittance terms, thus leading to the same tuning characteristics. In a waveguide–surfatron, the waveguide plunger corresponds to the tuning function of the surfatron's capacitive coupler, while the coaxial plunger plays the same role as that in a surfatron. Because of this similarity with the earlier surfatron, the present device bears the name waveguide–surfatron.

Figure 26 compares the measured and calculated tuning characteristics of a waveguide–surfatron having an outer diameter of coaxial section that is small compared with the width of the waveguide. The experimental data were obtained at 2.45 GHz, using a launcher based on a standard WR-430 rectangular waveguide, having a wide wall inside width 109.2 mm and a coaxial section with an outer conductor of 25.4 mm inner diameter (ID) and an inner conductor of 16 mm outer diameter (OD). The waveguide plunger is tuned for minimum reflected power at each position of the coaxial plunger. The full curve is a fit of the theoretical tuning characteristics to the experimental results. This fitted curve is plotted using equations (39) and (40) where the values of $r$ and of $x$ are determined from the two plunger positions at which there is zero reflected power in the measured tuning characteristic (for details see Moisan *et al* (1987)). Note the excellent agreement over a very large reflected power range, up to 80% of the incident power. The reason for such good results is that the incident power in the feed guide, for each coaxial plunger position, was adjusted to keep the amount of power delivered to the plasma $P_A = (P_I - P_R)$ constant. When instead $P_I$ is held constant, there are discrepancies in the tuning characteristic at large reflected powers, as pointed out in connection with figure 20 for the surfatron and figure 23 for the surfaguide.

The simple model for the waveguide–surfatron does not apply to launchers with a coaxial section designed to receive plasma tubes that are not small compared with the waveguide width. Nevertheless, it is important to be able to sustain plasma columns with diameters that are as large as possible at microwave frequencies. Thus some corresponding measured tuning characteristics are shown in figure 27, for a launcher based on the WR-430 waveguide with a coaxial section of outer conductor 89.4 mm ID and inner conductor 55.8 mm OD, and having an aperture that can accommodate tubes† of up to 52 mm OD. Note that the general shape of the tuning characteristic of the model is retrieved even in this case. With this tube diameter, depending on the position of the coaxial plunger, the

† Discharges in tubes of more than 80 mm OD have been sustained using the same waveguide section.

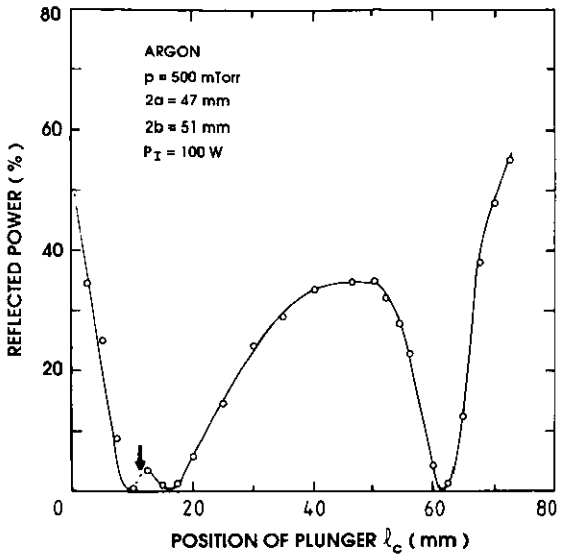


**Figure 27.** Measured tuning characteristic of a waveguide–surfatron having a large-diameter aperture, i.e. when the outer diameter of the coaxial section is not small compared with the width of the waveguide. The arrow indicates the plunger position where the surface wave changes from a pure $m = 1$ mode (left of the arrow) to an $m = 0$ mode. The latter is ill-defined in the present case because frequency times radius is relatively large.

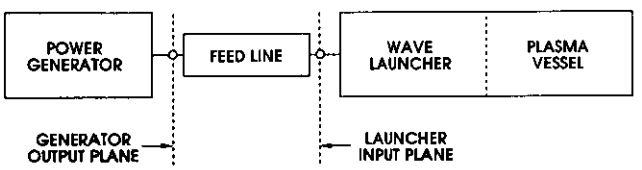


**Figure 28.** The essential parts of a typical SWD plasma source.

plasma column can be sustained either in an axially symmetric ($m = 0$) or in a dipolar ($m = 1$) mode wave. This subject is discussed by Moisan *et al* (1987) and in more detail by Margot-Chaker *et al* (1987, 1989).

## 5. Surface-wave plasma source set-ups

Figure 28 shows schematically the essential parts of a SWD plasma source. As a rule, however, an efficient and stable set-up also requires the elements shown in figure 29. These are the directional line and the power meter, which are needed to measure the power delivered to the launcher, and some auxiliary elements inserted between the generator and the launcher to improve the coupling efficiency and the stability of the plasma source. These elements are not all necessary in a given set-up but, if they are used, they must be connected in the order shown in figure 29. Also, they must be inserted into the feed line as close to the launcher input as possible so as to minimize power losses. This requirement becomes particularly important at microwave frequencies.

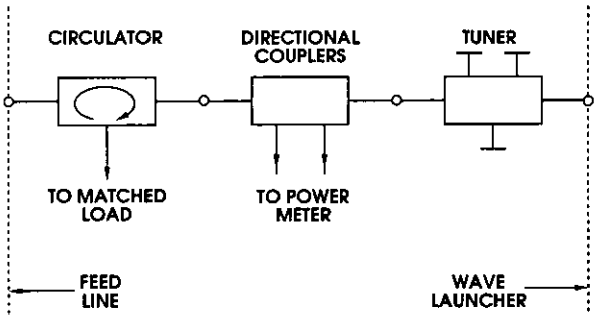


**Figure 29.** Set of auxiliary elements for an HF plasma source. The insertion sequence of the elements must be observed.

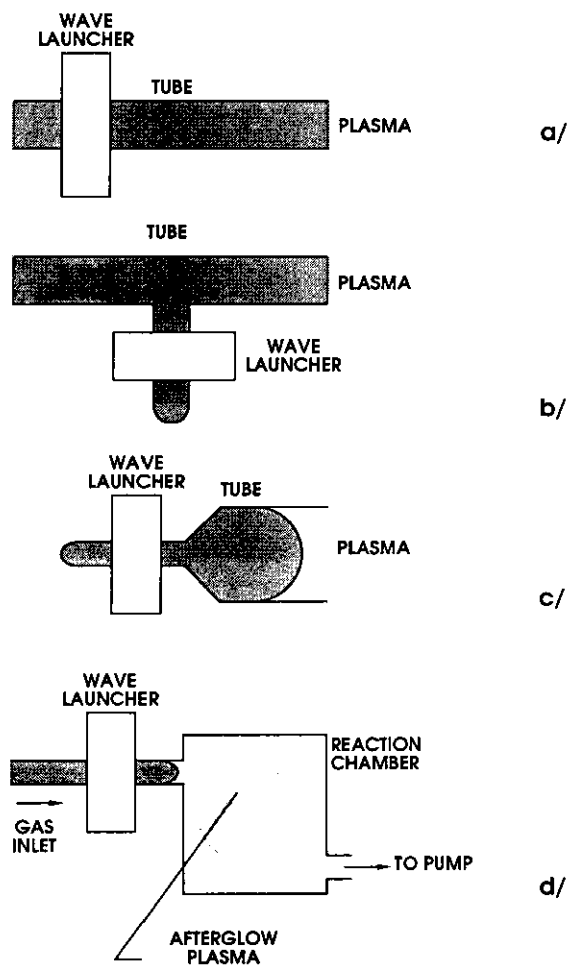


**Figure 30.** Examples of plasma vessels used in surface-wave plasma sources: cylindrical tube (*a*), symmetric **T** tube (*b*), tapered tube (*c*) and reaction chamber for use with an afterglow plasma (*d*).

All the above mentioned components that constitute the surface-wave plasma source, besides the launcher, are typical elements of microwave networks. For details on the related hardware and procedures see Hubert *et al* (1986). Other aspects of power feeding and measurement, in particular for microwave discharges, have been discussed by Jutte and Agterdenbos (1979), Outred (1980) and Outred and Hammond (1980).

We now discuss the discharge vessel since, as far as the discharge vessel shape is concerned, the use of surface waves to generate plasmas provides more flexibility than any other type of discharge. One reason is that the wave can be guided along the interface between the plasma and the surrounding medium. Another reason is that the volume of the discharge is easily controlled: it may be increased by simply raising the power delivered to the launcher.

To obtain a surface-wave sustained plasma, part of the plasma vessel must go into the launcher aperture†. The tube walls must be made of a low-loss dielectric (e.g. fused silica, glass, ceramic) to minimize the energy loss and the resulting overheating of the wall material. Nevertheless, some unavoidable wall heating results from energy transfer from the plasma particles and from radiation. This loss is particularly noticeable within the field applicator, where the metallic sleeve reduces the heat transport from the tube to the environment. Fortunately, for all the surface-wave launchers described in section 4, the launching gap opening can be used for directing compressed air onto the discharge tube.

The detailed design of the plasma vessel depends, of course, on its destination. Figure 30 shows some vessel configurations that are suitable for surface-wave discharges. The simplest and most commonly used one is the straight cylindrical tube shown in figure 30(*a*). Since we are dealing with guided waves, bending the tube does not prevent the generation of plasma (Moisan *et al* 1975). However, abrupt changes in tube shape or size cause some wave reflection and radiation into the surrounding space. The **T**-shaped vessel of figure 30(*b*), with the wave launcher located at the base of the **T**, can be used to sustain a plasma column that is symmetrical with respect to the junction. The length of this plasma can then be increased without disturbing the symmetry by simply raising the input power (Moutoulas *et al* 1985).

To operate large-diameter surface-wave discharges at high frequencies, a modified set-up shown schematically in figure 30(*c*) is recommended (Moisan and Zakrzewski 1985, 1989, 1990). The diameter of the usable section of the tube can be large relative to the wavelength and to the launcher dimensions, provided that it is tapered down at one end to a size that can be accommodated by the launcher. This design bypasses two limitations in the launching of surface waves in the $m = 0$ mode at high frequencies. One concerns the restriction on the launcher's aperture diameter which, for efficient operation, generally should not exceed a given fraction of the free space wavelength. The other limitation concerns the selective excitation of the $m = 0$ mode wave and was mentioned in section 3.2.2. In figure 30(*c*), the excited wave reaches the large-diameter section of the tube via the conical transition. The length of the transition is the result of a compromise: if the length is too small, the reflected wave power is excessive, and if the length is too large, there is too much power lost outside the usable section.

Figure 30(*d*) shows a plasma vessel of particular interest for set-ups in which the afterglow plasma is used in chemical reactions or surface processing. The active particles are generated within the discharge part of the vessel and from there they flow into the reaction chamber. Note that by increasing the HF input power to the launcher, the length of the plasma column increases and so does the residence time of particles through the discharge zone.

† One could also use a dielectric link, e.g. a Teflon tube, between the discharge tube and the wave launcher.

## 6. Conclusion

Surface-wave sustained discharges have allowed the expansion of the range of operating conditions and of plasma parameters available with other RF and microwave-induced discharges. For example, these new discharges offer the possibility of obtaining overdense plasmas in large discharge vessels or reaction chambers of shapes and dimensions that are not limited by the necessity of placing them inside RF or microwave circuits. Also, thanks to the characteristics of the surface wave sustaining the discharges (e.g. monomode wave propagation, weak dependence of the wave impedance on plasma parameters), the plasmas are reproducible, convenient to use, and quiescent. The broad range of wave frequencies and gas pressures over which these plasmas can be sustained proves to be advantageous in various applications as well as for a better understanding of RF and microwave discharge mechanisms in general.

The practical interest of these surface-wave discharges relies strongly on efficient and flexible wave launchers. In fact, the development of suitable wave launchers has been the main challenge of surface-wave plasma generation. The other parts of the plasma source are of a more or less conventional nature and may be dealt with by well established methods and procedures of RF and microwave engineering. It is because of this challenge that we have concentrated part of our research effort on that subject. This work has resulted in the development of the family of surface-wave plasma sources that we have reviewed in this paper.

## Acknowledgments

The authors are grateful to Professor P Lorrain and to Dr J Margot for valuable comments, and to J-E Samuel for drawing the figures. Thanks are also due to Messrs F Roy, R Grenier, R Lemay and R Martel who built the launchers. This work was supported in part by the Fonds pour la formation de chercheurs et l'aide à la recherche (FCAR) of Québec.

## References


Abdallah M H, Coulombe S, Mermet J M and Hubert J 1982 *Spectrochim. Acta* **37** B 583

Barlow H M and Brown J 1962 *Radio Surface-waves* (Oxford: Clarendon)

Beauchemin D, Hubert J and Moisan M 1986 *Appl. Spectrosc.* **40** 379

Beneking C and Anderer P 1987 *40th Annual Gaseous Electronics Conference* Conference abstracts EB-7; also 1988 *Bull. Am. Phys. Soc.* **33** 134

Bertrand L, Gagné J M, Bosisio R and Moisan M 1978 *IEEE J. Quant. Electron.* **14** 8

Bertrand L, Monchalin J P, Pitre R, Meyer M L, Gagné J M and Moisan M 1979 *Rev. Sci. Instrum.* **50** 708

Besner A, Hubert J and Moisan M 1988 *J. Anal. Atom. Spectrosc.* **3** 863

Bloyet E, Leprince P, Llamas Blasco M and Marec J 1981 *J. Physique Lett.* **83** A 391

Bollen W M, Waynant R W and Christensen C P 1985 *Naval Research Laboratory (Washington, DC) Memo Report* 5432

Chaker M, Moisan M and Zakrzewski Z 1986 *Plasma Chem. Plasma Process.* **6** 79

Chaker M, Nghiem P, Bloyet E, Leprince P and Marec J 1982 *J. Phys. Lett.* **43** L71

Chevrier G, Hanai T, Tran K C and Hubert J 1982 *Can. J. Chem.* **60** 898

Claude R, Moisan M, Wertheimer M R and Zakrzewski Z 1987 *Appl. Phys. Lett.* **50** 1979

Deruaz D and Mermet J M 1986 *Analysis* **14** 707

Ferreira C M 1983 *J. Phys. D: Appl. Phys.* **16** 1673

Ferreira C M 1986 *Radiative Processes in Discharge Plasmas* ed J M Proud and L H Luessen (New York: Plenum)

Ferreira C M and Loureiro J 1984 *J. Phys. D: Appl. Phys.* **17** 1175

Ferreira C M and Moisan M 1988 *Phys. Scr.* **38** 382

Galante L J, Selby M and Hieftje G M 1988 *Appl. Spectrosc.* **42** 559

Gamero A, Cotrino J, Sola A and Colomer V 1988 *J. Phys. D: Appl. Phys.* **21** 1275

Gamero A, Sola A, Cotrino J and Colomer V 1985 *XVII Int. Conf. Phenomena of Ionized Gases (Budapest)* ed J S Bakos and Z Sörlei *Contributed papers* vol 2, p 676

Ghose R N 1963 *Microwave Circuit Theory and Analysis* (New York: McGraw-Hill)

Granier A, Boisse-Laporte C, Leprince P, Marec J and Nghiem P 1987 *J. Phys. D: Appl. Phys.* **20** 204

Glaude V M M, Moisan M, Pantel R, Leprince P and Marec J 1980 *J. Appl. Phys.* **51** 5693

Hanai T, Coulombe S, Moisan M and Hubert J 1981 *Developments in Atomic Plasma Spectrochemical Analysis* ed R Barnes (London: Heyden)

Heald M A and Wharton C B 1965 *Plasma Diagnostics with Microwaves* (New York: Wiley)

Henry D, Hajlaoui Y, Arnal Y, Pantel R and Moisan M 1983 *Proc. Conf. Surface-wave in Plasmas (Sofia University)* ed I Zhelyazkov pp 292–5

Hollahan J R and Bell A T 1974 *Techniques and Applications of Plasma Chemistry* (New York: Wiley)

Hubert J, Moisan M and Ricard A 1979 *Spectrochim. Acta* **33** B 1

Hubert J, Moisan M and Zakrzewski Z 1986 *Spectrochim. Acta* **41** B 205

Ingold J H 1978 *Gaseous Electronics* vol 1 ed M N Hirsch and H J Oskam (New York: Academic)

Jutte B A H G and Agterdenbos J 1979 *Spectrochim. Acta* **34** B 133

Kerns D M and Beatty R W 1967 *Basic Theory of Waveguide Junctions* (Oxford: Pergamon)

Levitskiy S M and Baranchuk N S 1961 *Izv. VUZ Radiofiz.* **4** 1078

Levy D 1990 *43rd Annual Gaseous Electronics* Conference abstracts GB-2

Leprince P, Matthieussent G and Allis W P 1971 *J. Appl. Phys.* **42** 412

Llamas M, Colomer V and Rodriguez Vidal M 1985 *J. Phys. D: Appl. Phys.* **18** 2169

Loncar G, Musil J and Bardos L 1980 *Czech. J. Phys.* B **30** 688

MacDonald A D and Tentenbaum S J 1978 *Gaseous Electronics* ed M N Hirsch and H J Oskam (New York: Academic) ch 3

Marec J, Bloyet E, Chaker M, Leprince P and Nghiem P 1982 *Electrical Breakdown and Discharges in Gases* ed E E Kunhardt and L H Luessen (New York: Plenum)

Margot J, Moisan M and Ricard A 1991 *Appl. Spectrosc.* **45** 260

Margot-Chaker J, Moisan M, Chaker M, Glaude V M M, Lauque P, Paraszczak J and Sauvé G 1989 *J. Appl. Phys.* **66** 4134

Margot-Chaker J, Moisan M, Chaker M, Paraszczak J and Sauvé G 1987 *Contributed Papers from XVIII Int. Conf. on Phenomena in Ionized Gases* vol 4 (Bristol: Adam Hilger) p 854

Moisan M, Barbeau C, Claude R, Ferreira C M, Margot J, Paraszczak J, Sá A B, Sauvé G and Wertheimer M 1991 *J. Vac. Sci. Technol.* B **9** 8

Moisan M, Beaudry C, Bertrand L, Bloyet E, Gagné J M, Leprince P, Marec, J, Mitchel G, Ricard A and Zakrzewski Z 1976 *Inst. Elec. Eng. Conf. Pub.* **143** p 382

Moisan M, Beaudry C and Leprince P 1974 *Phys. Lett.* **50** A 125

—— 1975 *IEEE Trans. Plasma Sci.* **3** 55

Moisan M, Chaker M, Zakrzewski Z and Paraszczak J 1987 *J. Phys. E: Sci. Instrum.* **20** 1356

Moisan M, Ferreira C M, Hajlaoui Y, Henry D, Hubert J, Pantel R, Ricard A and Zakrzewski Z 1982b *Revue Phys. Appl.* **17** 707

Moisan M, Leprince P, Beaudry C and Bloyet E 1977 *US Patent* 4,049,940

Moisan M, Pantel R and Hubert J 1990 *Contrib. Plasma Phys.* **80** 293

Moisan M, Pantel R, Hubert J, Bloyet E, Leprince P, Marec J and Ricard A 1979b *J. Microw. Power* **14** 57

Moisan M, Shivarova A and Trivelpiece A W 1982a *Plasma Phys.* **24** 1331

Moisan M and Zakrzewski Z 1985 in *Contributed papers from XVII Int. Conf. on Phenomena in Ionized Gases (Budapest)* ed S Bakos and Z Sörlei *Contributed papers* vol 2, p 712

—— 1986 *Radiative Processes in Discharge Plasmas* ed J M Proud and L H Luessen (New York: Plenum)

—— 1987 *Rev. Sci. Instrum.* **58** 1895

—— 1988 *Canadian Patent* 1,246,762

—— 1989 *US Patent* 4,810,933

—— 1990 *US Patent* 4,906,898

Moisan M, Zakrzewski Z and Pantel R 1979a *J. Phys. D: Appl. Phys.* **12** 219

Moisan M, Zakrzewski Z, Panel R and Leprince P 1984 *IEEE Trans. Plasma Sci.* **12** 203

Moutoulas C, Moisan M, Bertrand L, Hubert J, Lachambre J L and Ricard A 1985 *Appl. Phys. Lett.* **46** 323

Nowakowska H, Zakrzewski Z and Moisan M 1990 *J. Phys. D: Appl. Phys.* **22** 789

Outred M 1980 *Spectrochim. Acta* **35** B 447

Outred M and Hammond C B 1980 *J. Phys. D: Appl. Phys.* **13** 1609

Paquin L, Masson D, Wertheimer M and Moisan M 1985 *Can. J. Phys.* **63** 831

Paraszczak J, Heindenreich J, Hatzakis M and Moisan M 1985 *Microelectron. Eng.* **3** 397
Pomathiod L, Michau J L and Hamelin M 1988 *Rev. Sci. Instrum.* **59** 2409
Ricard A, Barbeau C, Besner A, Hubert J, Margot-Chaker J, Moisan M and Sauvé G 1988 *Can. J. Phys.* **66** 740
Rivière B, Mermet J M and Deruaz D 1987 *J. Anal. Atom. Spectrosc.* **2** 705
Sauvé G, Moisan M, Paraszczak J and Heindenreich J 1988 *Appl. Phys. Lett.* **53** 470
Selby M and Hieftje G M 1987 *Spectrochim. Acta* **42** B 285
Selby M, Rezaaiyaan R and Hieftje G M 1987 *Appl. Spectrosc.* **41** 749
Self S A and Ewald H N 1966 *Phys. Fluids* **9** 2486
Shivarova A and Zhelyazkov I 1978 *Plasma Phys.* **20** 1049
Taillet J 1969 *Am. J. Phys.* **37** 423
Trivelpiece A W 1967 *Slow-Wave Propagation in Plasma Waveguides* (San Francisco: San Francisco University Press)
Trivelpiece A W and Gould R W 1959 *J. Appl. Phys.* **30** 1784
Tuma D R 1970 *Rev. Sci. Instrum.* **41** 1519
Waynant R W, Bollen W M and Christensen C P 1985 *Bull. Am. Phys. Soc.* **30** 136
Zakrzewski Z 1983 *J. Phys. D: Appl. Phys.* **16** 171
Zakrzewski Z and Moisan M 1986 *Surface-waves in Plasmas and Solids* ed S Vukovic (Singapore: World Scientific) pp 440–66
Zakrzewski Z, Moisan M, Glaude V M M, Beaudry C and Leprince P 1977 *Plasma Phys.* **19** 77
Zhelyazkov I and Benova E 1989 *J. Appl. Phys.* **66** 1641
Zhelyazkov I, Benova E and Atanassov V 1986 *J. Appl. Phys.* **59** 1466